MAX-PLANCK-INSTITUT
FÜR PLASMAPHYSIK

Pedestal turbulence in AUG and JET from a global gyrokinetic perspective

Leonhard Leppin[1], Tobias Görler[1], Marco Cavedon[2], Mike Dunne[1], Elisabeth Wolfrum[1], S. Saarelma[3], L. Frassinetti[4], J. Hobirk[1], Frank Jenko[1], ASDEX Upgrade Team[5] and JET Contributors[6]

[1]*Max Planck Institute for Plasma Physics, Garching b. München, Germany*
[2]*Dept. of Physics "G. Occhialini", University of Milano-Bicocca, Milan, Italy*
[3]*CCFE, Culham Science Center, Abingdon OX14 3DB, United Kingdom of Great Britain and Northern Ireland*
[4]*Division of Fusion Plasma Physics, KTH Royal Institute of Technology, SE-10691 Stockholm, Sweden*
[5]*See author list of U. Stroth et al. 2022 Nucl. Fusion 62 042006*
[6]*See Mailloux et al 2022 (https://doi.org/10.1088/1741-4326/ac47b4) for the JET Contributors*

This work has been carried out within the framework of the EUROfusion Consortium, funded by the European Union via the Euratom Research and Training Programme (Grant Agreement No 101052200 — EUROfusion). Views and opinions expressed are however those of the author(s) only and do not necessarily reflect those of the European Union or the European Commission. Neither the European Union nor the European Commission can be held responsible for them.

Overview

Small-scale turbulence in pedestal

- **Instability analysis**
- **Heat flux simulations (local & global)**

- **2 ELMy H-modes: ASDEX Upgrade**
  JET hybrid scenario

Tool: GENE
genecode.org

with upgrade for global,
nonlinear, experimental β simulations

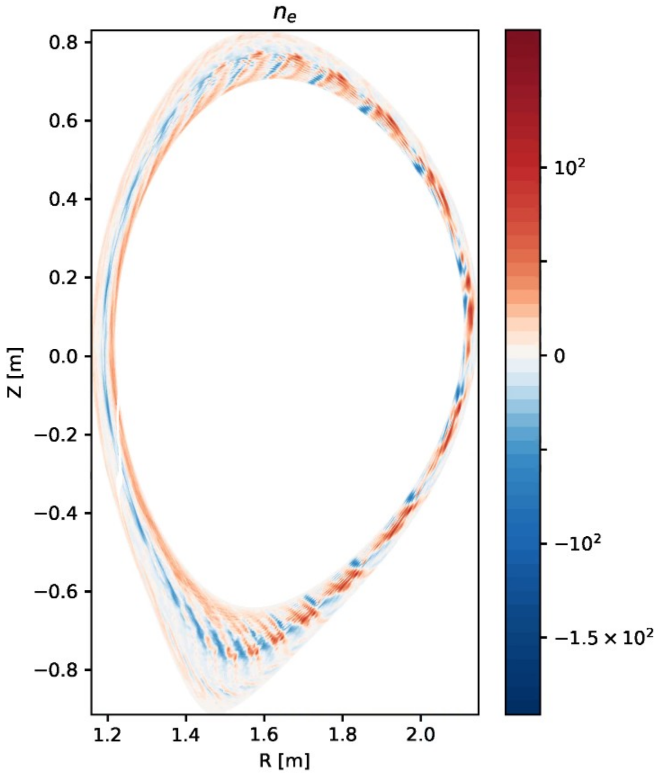

Goal: Identify dominant turbulence mechanisms & how they change across pedestal

Outline

Part I: Upgrade of global, electromagnetic GENE

Part II & III: Turbulence characterization in pedestals of AUG & JET

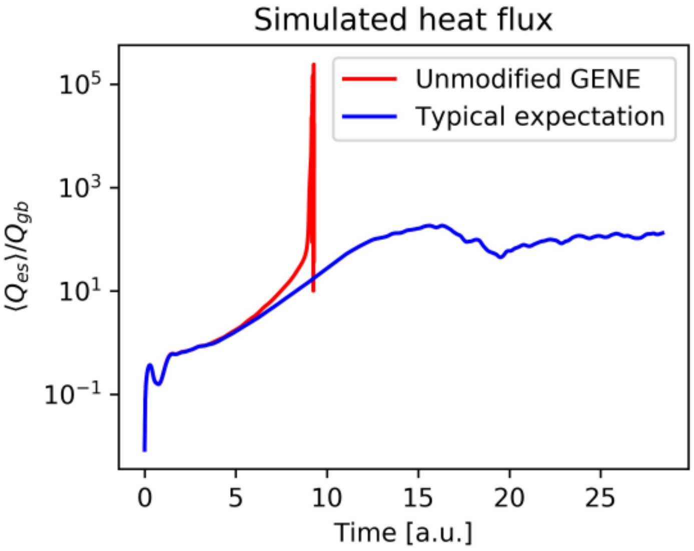

Simulation diverges!

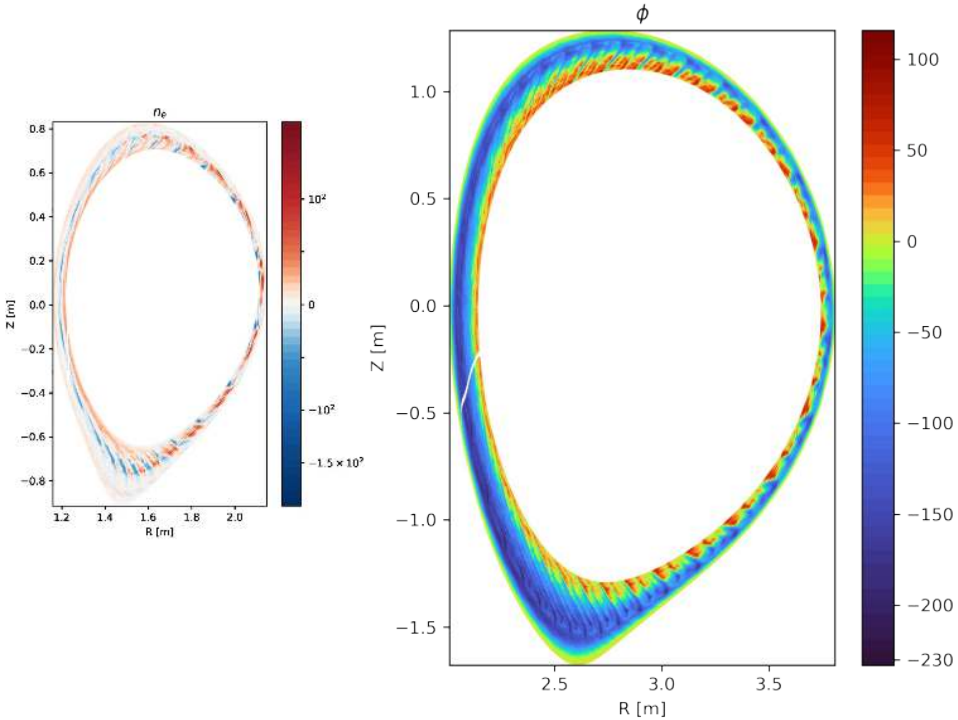

Types of simulations

All presented simulations:

- gyrokinetic
- gradient-driven
- δf
- electromagnetic (ϕ_1,$A_{||,1}$ but no $B_{||,1}$)
- collisions
- true m_e/m_i

Depending on aim:

- local, linear → instability characterization
- local, nonlinear → electron-scale turbulence/fluxes
- global, nonlinear → ion-scale turbulence/fluxes

Part I:
Upgrade of global, electromagnetic GENE

Gyrokinetic equation

Vlasov equation: Time evolution of the distribution of gyrocenters *F* in 5D phase space

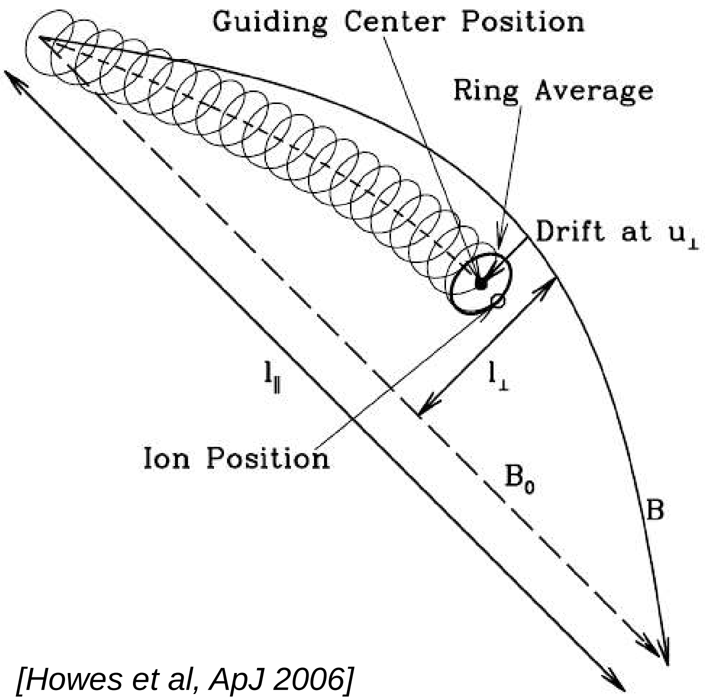

[Howes et al, ApJ 2006]

$$\frac{\partial F}{\partial t} + \frac{\partial \boldsymbol{X}}{\partial t} \cdot \boldsymbol{\nabla} F + \frac{\partial v_{||}}{\partial t} \frac{\partial F}{\partial v_{||}} = 0$$

Drifts:

$$\frac{\partial \boldsymbol{X}}{\partial t} = v_{||} \hat{\boldsymbol{b}} + \frac{B}{B_{||}^*} (\boldsymbol{v}_{\boldsymbol{\nabla} B} + \boldsymbol{v}_\chi + \boldsymbol{v}_c)$$

Parallel acceleration:

Parallel magnetic vector potential

$$\frac{\partial v_{||}}{\partial t} = - \frac{1}{m v_{||}} \frac{\partial \boldsymbol{X}}{\partial t} \cdot \left(\mu \boldsymbol{\nabla} (B + \bar{B}_{1||}) + q \boldsymbol{\nabla} \bar{\phi}_1 \right) - \frac{q}{mc} \frac{\partial \bar{A}_{1||}}{\partial t}$$

In standard GENE

- **Some intermediate steps:**

  … normalize ….

  … split distribution into background and flucuating part „delta-f approach“: $F = F_0 + f_1$

  … transform to field- aligned coordinates …

- **Collect all time derivatives on left hand side of equation for explicit time solver:**

$$\frac{\partial f_1}{\partial t} - \frac{q}{mc}\frac{\partial \bar{A}_{1||}}{\partial t}\frac{\partial F_0}{\partial v_{||}} = \ldots$$

- **Introduce new distribution function g:** $g_1 := f_1 - \frac{q}{mc}\bar{A}_{1||}\frac{\partial F_0}{\partial v_{||}}$ ➡ $\frac{\partial g_1}{\partial t} = \ldots$

  – **Works generally well,**
    but tends to be unstable in global, nonlinear, electromagnetic simulations

Upgrade

- **following the proof-of-principle by P. Crandall [1] based on [2]:**
  - **keep unmodified distribution *f*** $$\frac{\partial f_1}{\partial t} = \frac{q}{mc}\frac{\partial \bar{A}_{1||}}{\partial t}\frac{\partial F_0}{\partial v_{||}} + R_b$$

    All remaining terms
  - **use Ampere's law** $\nabla_\perp^2 A_{||} = -\frac{4\pi}{c} j$ **to derive a field equation for** $E_{||}^{\text{ind}} = -\frac{1}{c}\frac{\partial A_{||}}{\partial t}$

$$\left(\nabla_\perp^2 + \frac{4\pi}{c^2}\sum_b \frac{q_b^2}{m_b}\int d^3v \mathcal{G}^\dagger v_{||}\frac{\partial F_b}{\partial v_{||}}\mathcal{G}\right) E_{||}^{\text{ind}} = \frac{4\pi}{c^2}\sum_b q_b \int d^3v \mathcal{G}^\dagger \{v_{||} R_b\}$$

  - **solve numerically**

[1] Crandall, 2019, PhD Thesis, UCLA
[2] Reynders, 1993, PhD Thesis, Princeton

Changes in GENE model

$$
\begin{aligned}
\frac{\partial \hat{f}_{1\sigma}}{\partial \hat{t}} =\; & \frac{1}{\hat{C}}\frac{\hat{B}_0}{\hat{B}^*_{0||}}\left[\hat{\omega}_{n\sigma} + \hat{\omega}_{T\sigma}\left(\frac{\hat{v}_{||}^2 + \hat{\mu}\hat{B}_0}{\hat{T}_{0\sigma}/\hat{T}_{0\sigma}(x_0)} - \frac{3}{2}\right)\right]\hat{F}_{0\sigma}\hat{v}_{T\sigma}(x_0)\hat{v}_{||}\partial_{\hat{y}}\hat{\bar{A}}_{1||} \\
& - \left\{\frac{1}{\hat{C}}\frac{\hat{B}_0}{\hat{B}^*_{0||}}\left[\hat{\omega}_{n\sigma} + \hat{\omega}_{T\sigma}\left(\frac{\hat{v}_{||}^2 + \hat{\mu}\hat{B}_0}{\hat{T}_{0\sigma}/\hat{T}_{0\sigma}(x_0)} - \frac{3}{2}\right)\right]\hat{F}_{0\sigma}\right. \\
& \left. + \frac{\hat{B}_0}{\hat{B}^*_{0||}}\frac{\hat{T}_{0\sigma}(x_0)}{\hat{T}_{0\sigma}}\frac{\hat{\mu}\hat{B}_0 + 2\hat{v}_{||}^2}{\hat{B}_0}\hat{K}_y\hat{F}_{0\sigma} + \frac{\hat{B}_0}{\hat{B}^*_{0||}}\frac{\hat{T}_{0\sigma}(x_0)}{\hat{T}_{0\sigma}}\frac{\hat{v}_{||}^2}{\hat{C}}\beta_{\mathrm{ref}}\frac{\hat{p}_0}{\hat{B}_0^2}\hat{\omega}_p\hat{F}_{0\sigma}\right\}\partial_{\hat{y}}\hat{\bar{\phi}}_1 \\
& - \frac{\hat{B}_0}{\hat{B}^*_{0||}}\frac{\hat{T}_{0\sigma}(x_0)}{\hat{T}_{0\sigma}}\frac{\hat{\mu}\hat{B}_0 + 2\hat{v}_{||}^2}{\hat{B}_0}\hat{K}_x\hat{F}_{0\sigma}\partial_{\hat{x}}\hat{\bar{\phi}}_1 \\
& - \frac{\hat{B}_0}{\hat{B}^*_{0||}}\frac{\hat{T}_{0\sigma}(x_0)}{\hat{q}_\sigma}\frac{\hat{\mu}\hat{B}_0 + 2\hat{v}_{||}^2}{\hat{B}_0}\hat{K}_x\partial_{\hat{x}}\hat{f}_{1\sigma} \\
& - \left\{\frac{\hat{B}_0}{\hat{B}^*_{0||}}\frac{\hat{T}_{0\sigma}(x_0)}{\hat{q}_\sigma}\frac{\hat{\mu}\hat{B}_0 + 2\hat{v}_{||}^2}{\hat{B}_0}\hat{K}_y + \frac{\hat{B}_0}{\hat{B}^*_{0||}}\frac{\hat{T}_{0\sigma}(x_0)}{\hat{q}_\sigma}\frac{\hat{v}_{||}^2}{\hat{C}}\beta_{\mathrm{ref}}\frac{\hat{p}_0}{\hat{B}_0^2}\hat{\omega}_p\right\}\partial_{\hat{y}}\hat{f}_{1\sigma} \\
& - \hat{v}_{T\sigma}(x_0)\frac{\hat{C}}{J\hat{B}_0}\hat{v}_{||}\left(\partial_{\hat{z}}\hat{F}_{0\sigma} + \frac{\hat{q}_\sigma}{\hat{T}_{0\sigma}}\hat{F}_{0\sigma}\partial_{\hat{z}}\hat{\bar{\phi}}_1 + \frac{\hat{T}_{0\sigma}(x_0)}{\hat{T}_{0\sigma}}\hat{F}_{0\sigma}\hat{\mu}\partial_{\hat{z}}\hat{\bar{B}}_{1||}\right) \\
& + \frac{\hat{v}_{T\sigma}(x_0)}{2}\frac{\hat{C}}{J\hat{B}_0}\partial_{\hat{z}}\hat{B}_0\frac{\partial\hat{F}_{1\sigma}}{\partial\hat{v}_{||}} + \frac{\hat{B}_0}{\hat{B}^*_{0||}}\frac{1}{\hat{C}}\left(-\partial_{\hat{x}}\hat{\bar{\xi}}_1\partial_{\hat{y}}\hat{f}_{1\sigma} + \partial_{\hat{y}}\hat{\bar{\xi}}_1\partial_{\hat{x}}\hat{f}_{1\sigma} + \hat{q}_\sigma\frac{\hat{F}_{0\sigma}}{\hat{T}_{0\sigma}}\left(-\partial_{\hat{x}}\hat{\bar{\xi}}_1\partial_{\hat{y}}\hat{\bar{\phi}}_1 + \partial_{\hat{y}}\hat{\bar{\xi}}_1\partial_{\hat{x}}\hat{\bar{\phi}}_1\right)\right) \\
& + \frac{\hat{B}_0}{\hat{B}^*_{0||}}\hat{F}_{0\sigma}\frac{\hat{T}_{0\sigma}(x_0)}{\hat{q}_\sigma}\frac{\hat{\mu}\hat{B}_0 + 2\hat{v}_{||}^2}{\hat{B}_0}\hat{K}_x\left[\hat{\omega}_{n\sigma} + \hat{\omega}_{T\sigma}\left(\frac{\hat{v}_{||}^2 + \hat{\mu}\hat{B}_0}{\hat{T}_{0\sigma}/\hat{T}_{0\sigma}(x_0)} - \frac{3}{2}\right)\right] \\
& + \frac{\hat{q}_\sigma}{\hat{T}_{0\sigma}}\hat{v}_{||}\hat{F}_{0\sigma}\bar{E}_{\mathrm{ind}||}
\end{aligned}
$$

Changes for new f-version marked yellow

Verification of implementation

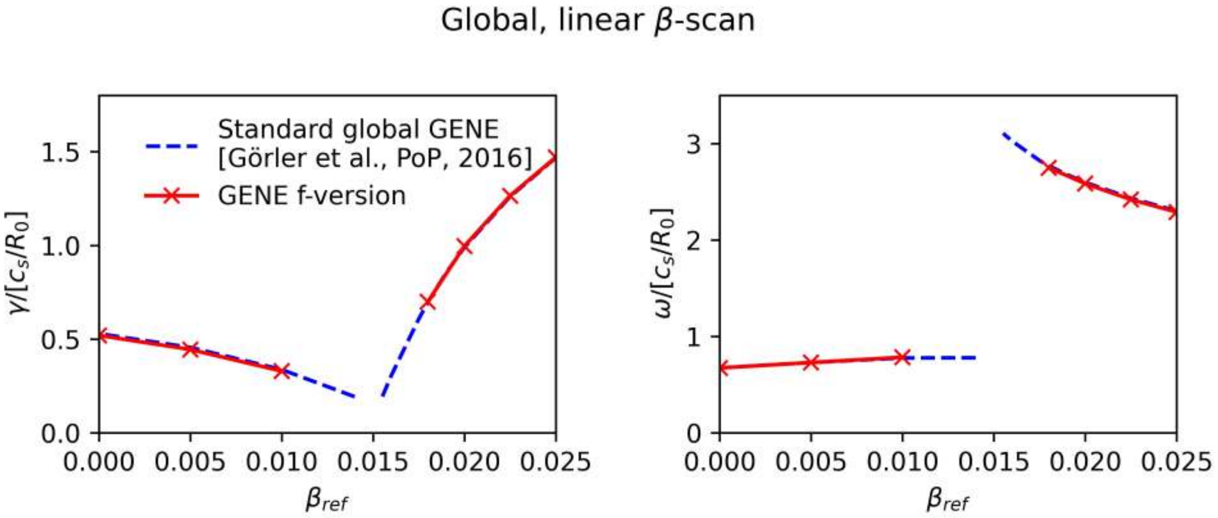

→ Upgrade agrees with global, linear results of code benchmark

Implementation details

- **Implementation of f-version:**
  - **fully integrated into GENE master branch (one switch in input parameters)**
  - **Compatible with block-structured velocity grids:**
    - **speed up < x10 (depending on profiles)**
  - **requires additional field equation for E_{ind} and nonlinear term**
    - **ca. 30% more computationally expensive**

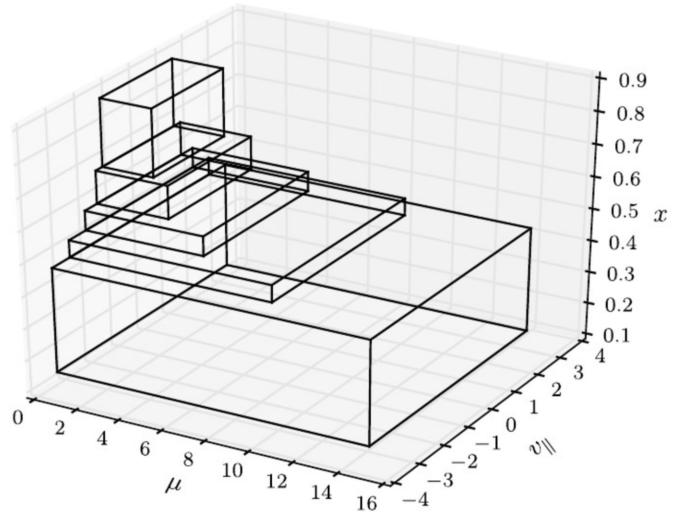

[D Jarema et al, CPC, 2017]

Conclusions

I. **f-version upgrade of GENE code enables stable global, nonlinear, electromagnetic pedestal simulations**

Part II:
Turbulence characterization in AUG pedestal

ELMy H-mode pedestal from AUG

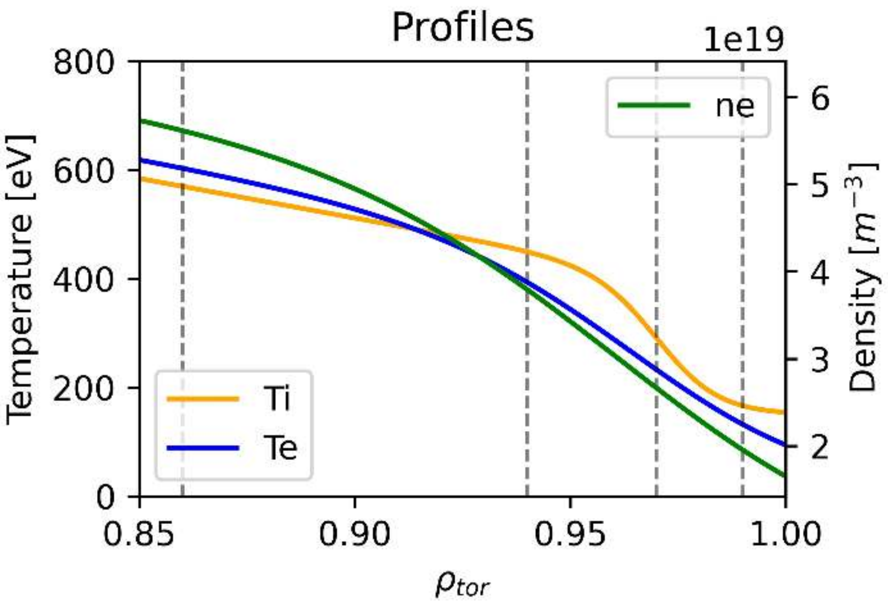

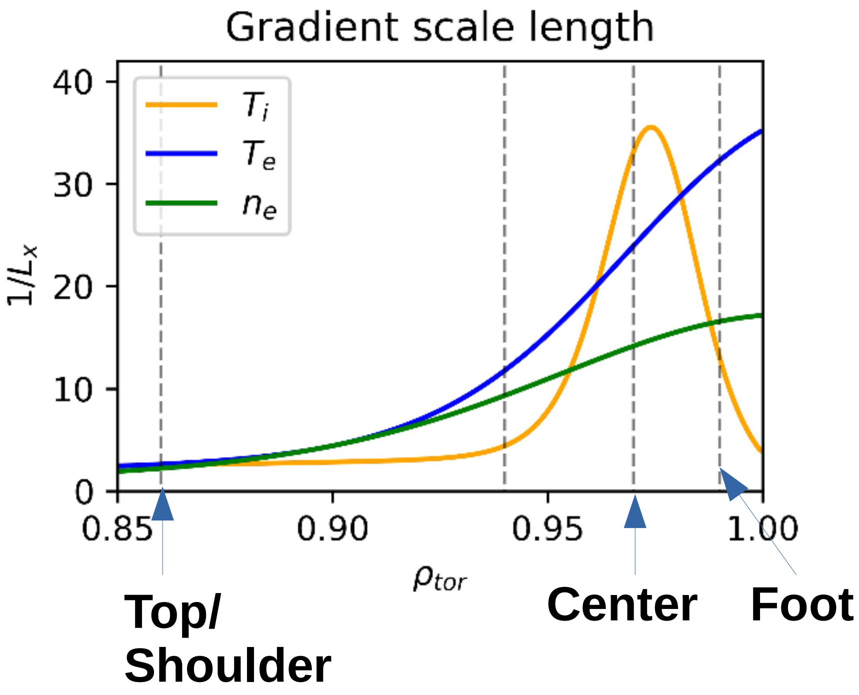

- Asdex Upgrade #31529 *[1]*
- NBI + ECRH heating, P_{tot} ~ 8.7MW
- On-axis B-field -2.5 T, plasma current 1MA
- ELM- synchronized profiles (6ms after ELM, almost pre-ELM)
- pressure-constrained magnetic equilibrium

[1] Cavedon et al., PPCF, 2017

Linear instabilities

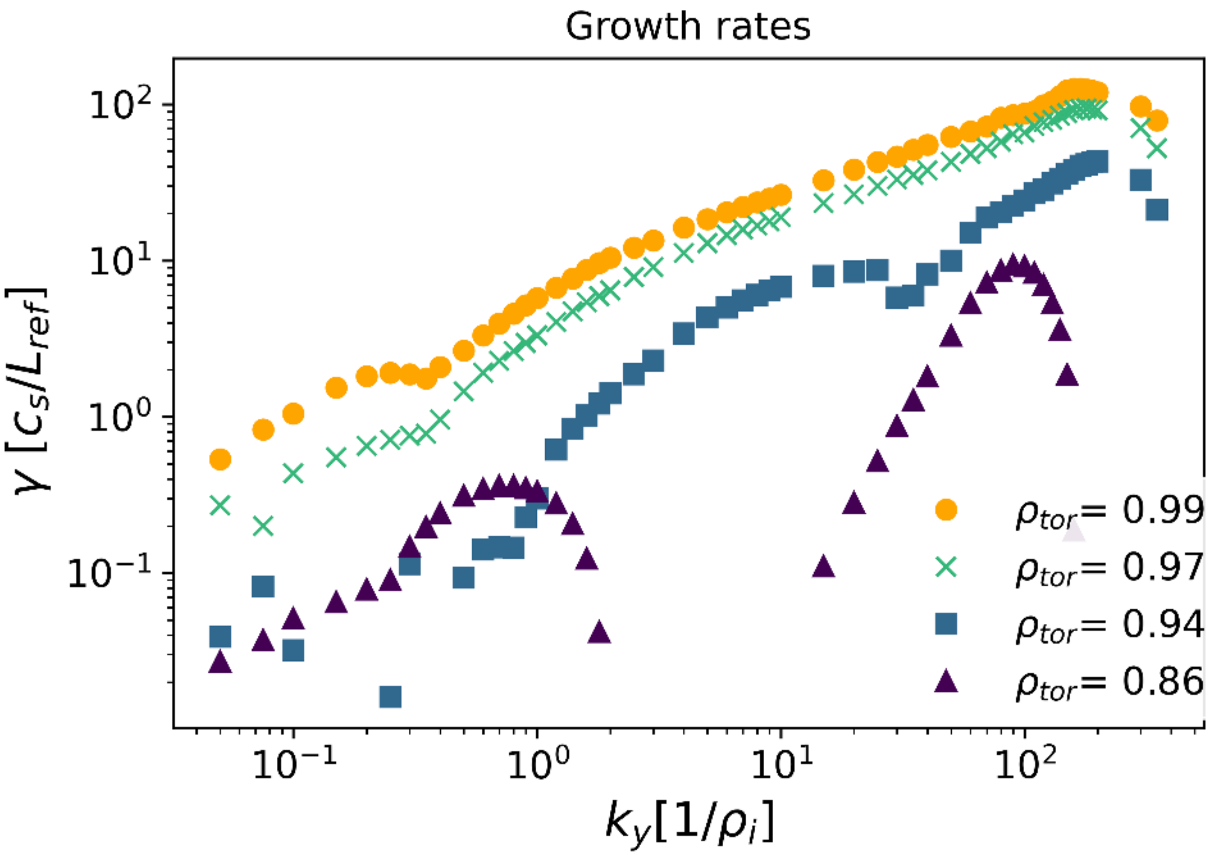

Linear instabilities

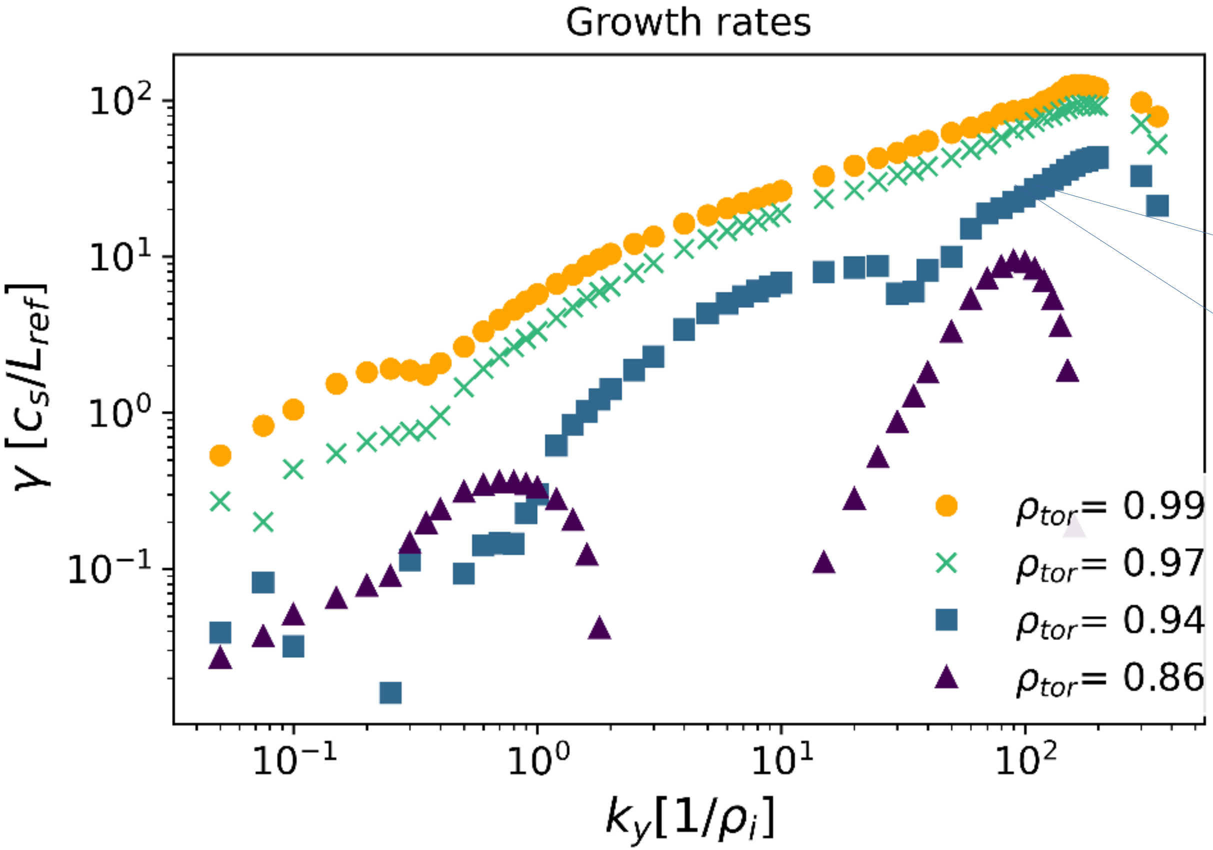

Growth rates are max. over k_x at outboard midplane.
e.g. ρ_{tor} = 0.97, k_y = 110

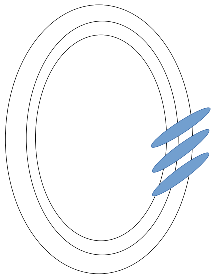

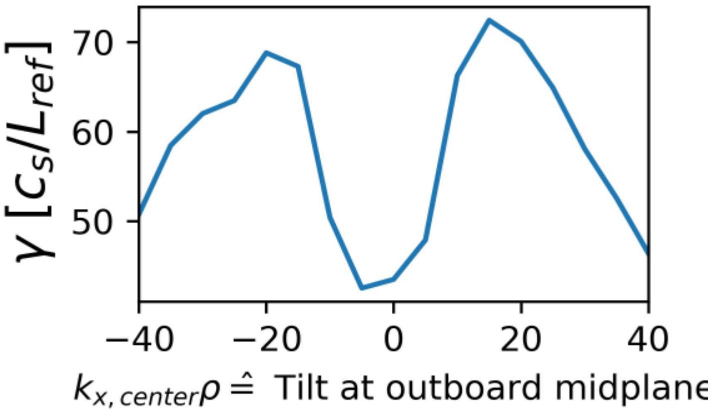

Linear instabilities

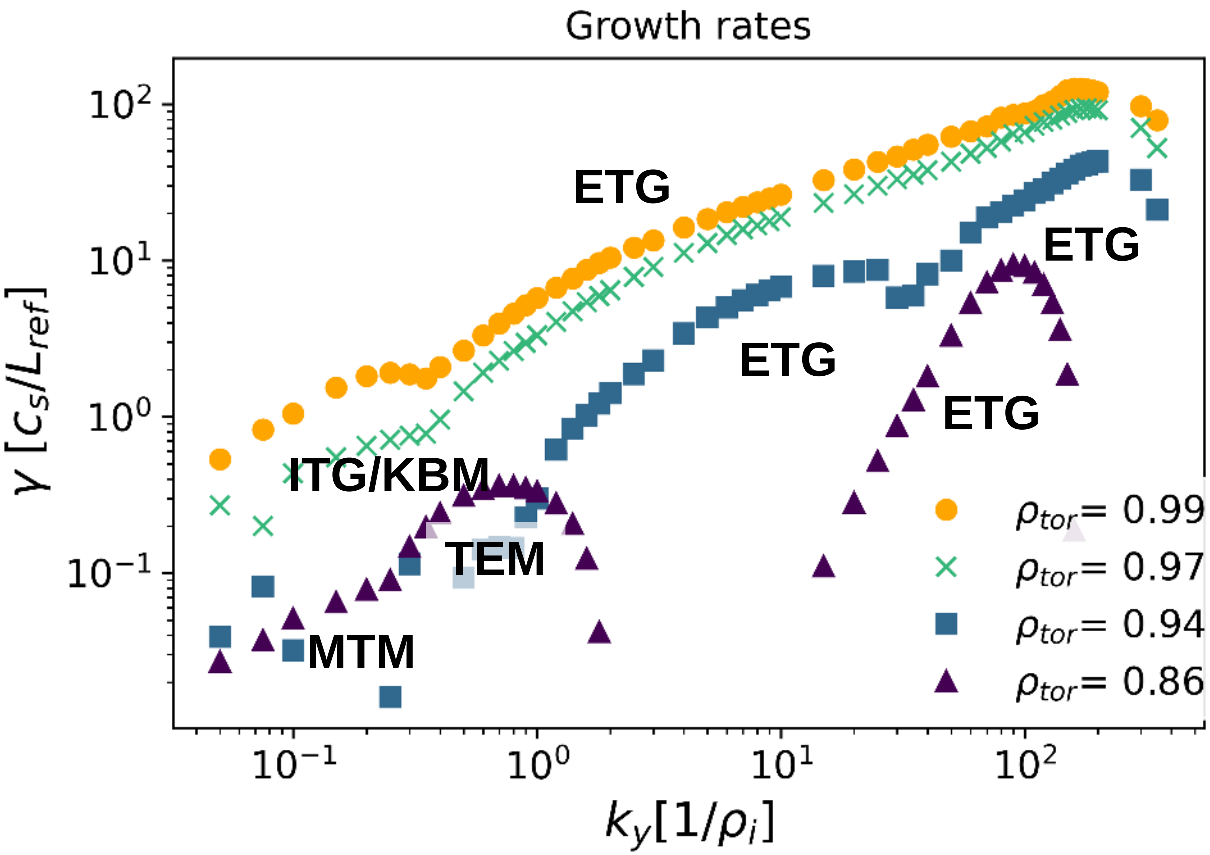

- **Ion scales:**
  Top: TEM/MTM → Center: ITG/KBM
  Growth rate gap at ρ_{tor}= 0.94 (blue)

- **Electron scales:** ETG
  with additional intermediate k_y
  ETG instabilities towards pedestal center

- Overall growth rates increase
  towards pedestal center/ foot

TEM: Trapped Electron Mode
MTM: Micro Tearing Mode
ETG: Electron Temperature Gradient Mode
ITG: Ion Temperature Gradient Mode

Pressure and magnetic shear effect

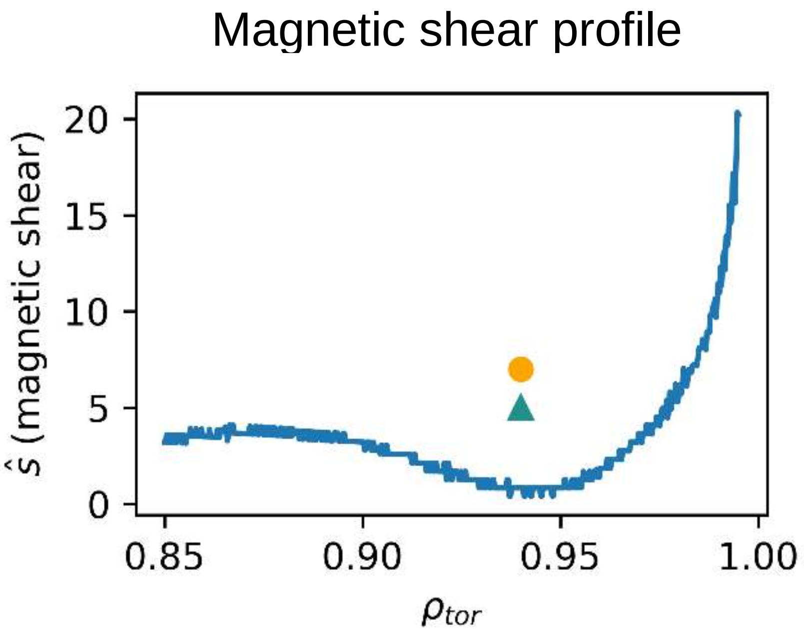

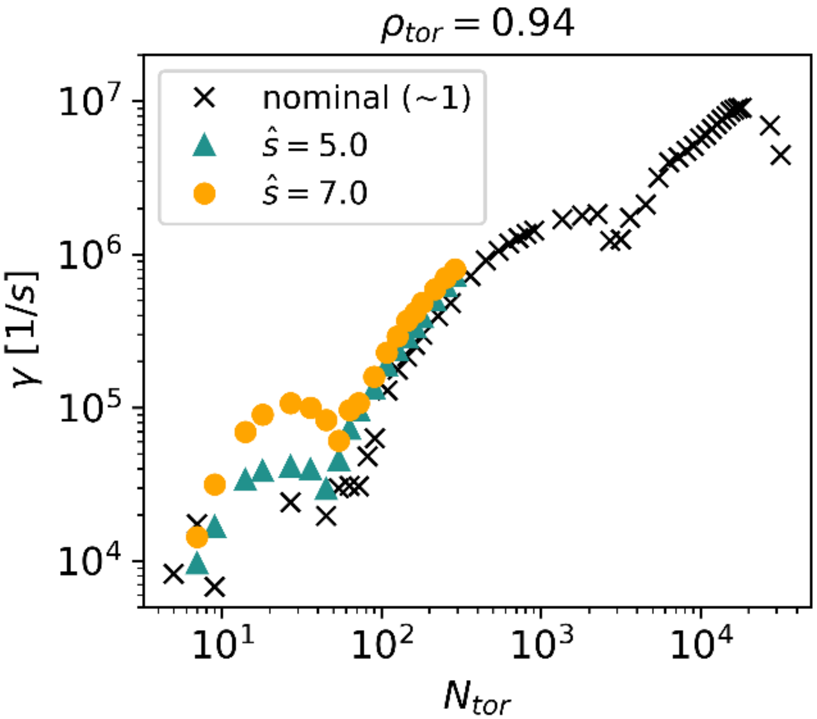

At ρ_{tor} = 0.94 ion scale growth rates increase with increasing(!) magnetic shear

→ In 2nd stability region at nominal parameters

Linear instabilities

Nonlinear simulation domains in k_y:

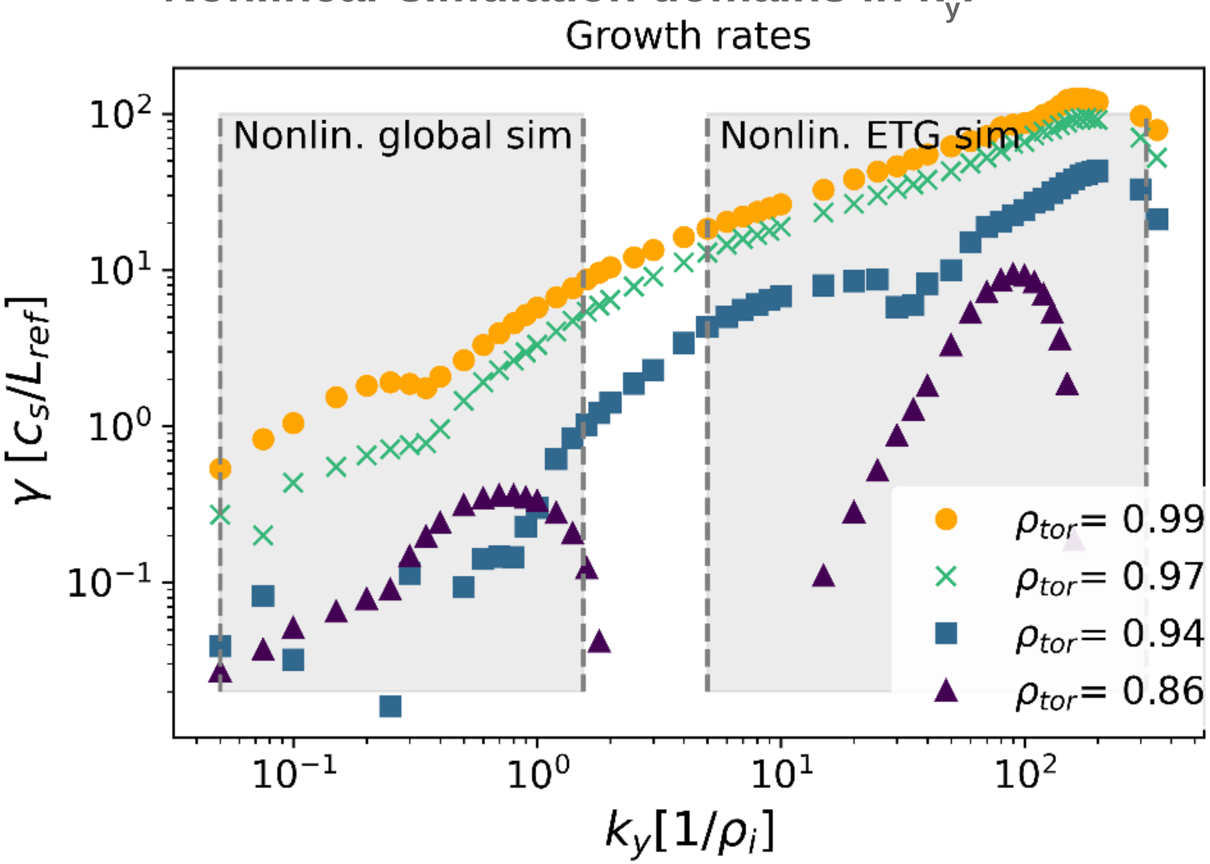

- **Ion scales:**
  Top: TEM/MTM → Center: ITG/KBM
  Growth rate gap at ρ_{tor}= 0.94 (blue)

- **Electron scales:** ETG
  with additional intermediate k_y
  ETG instabilities towards pedestal center

- Overall growth rates increase
  towards pedestal center/ foot

TEM: Trapped Electron Mode
MTM: Micro Tearing Mode
ETG: Electron Temperature Gradient Mode
ITG: Ion Temperature Gradient Mode

Global, ion scale: Turbulent heat fluxes

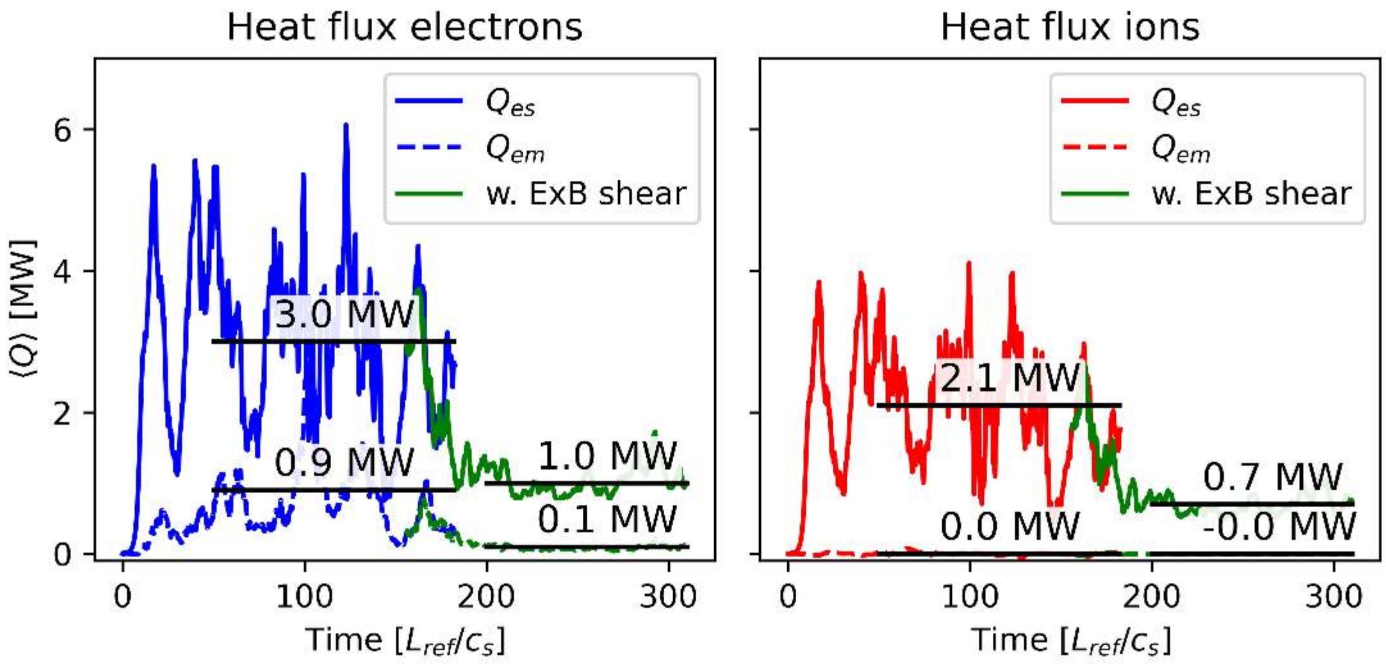

- Electrostatic heat flux dominates
- ExB shear reduces heat fluxes by ~3

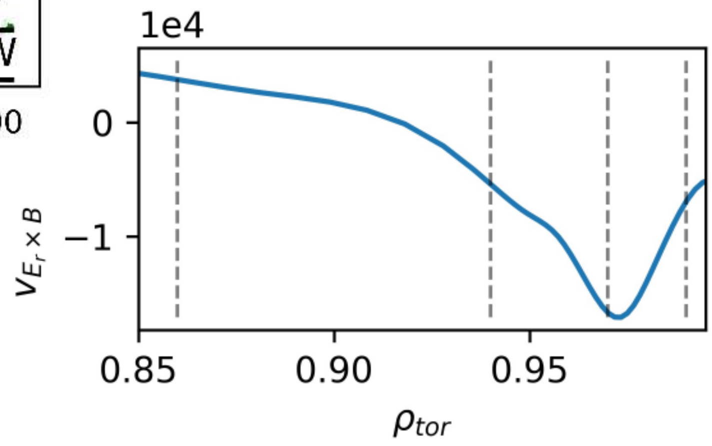

Connecting linear instabilities and nonlinear modes

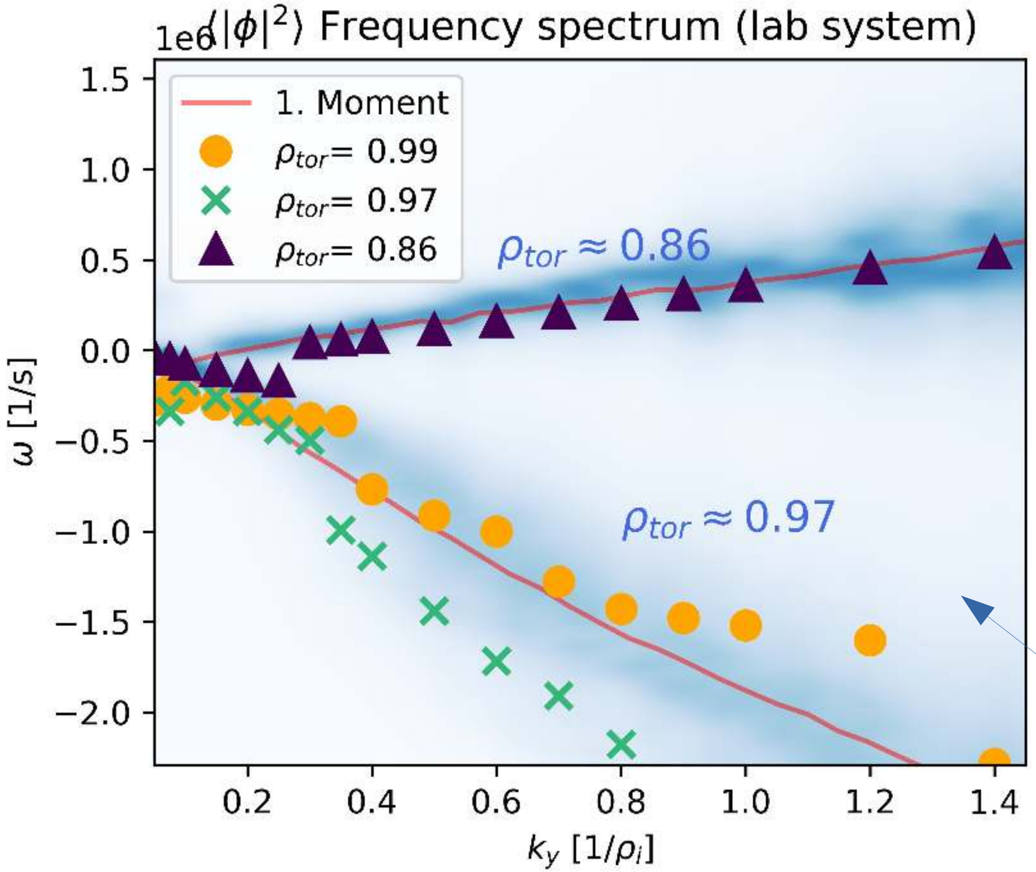

- Linear frequencies remain present at pedestal top and center
  → encouraging for quasi-linear models in pedestal

- MTM is suppressed in global, nonlinear simulations

Blue background: Nonlinear frequency distribution

Connecting linear instabilities and nonlinear modes: Cross phases

Pedestal top

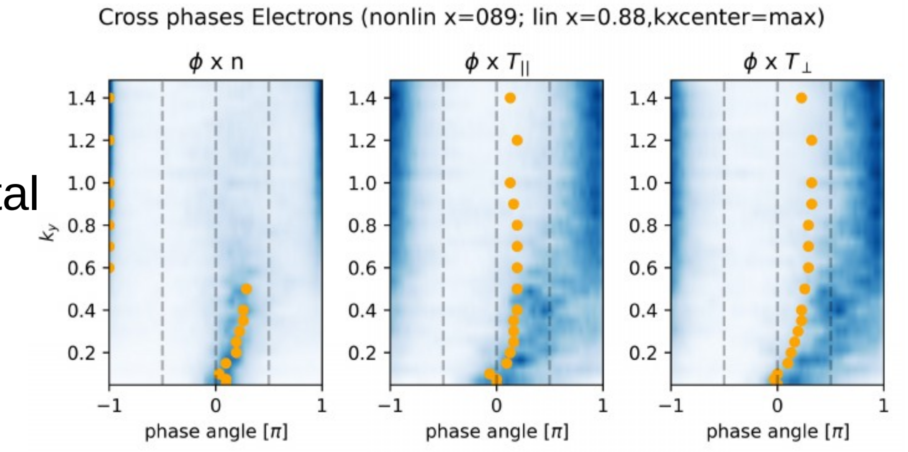

Pedestal center

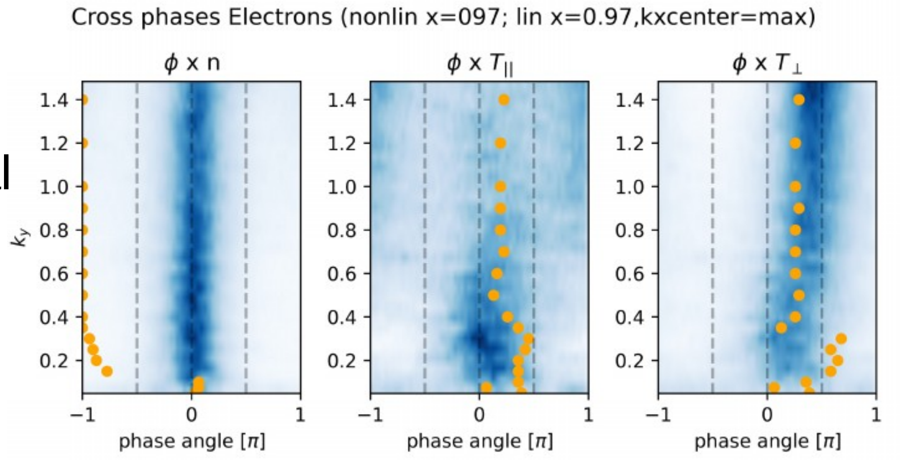

→ Cross phases support that some linear mode characteristics survive in particular at pedestal top

Turbulent heat flux structure in pedestal

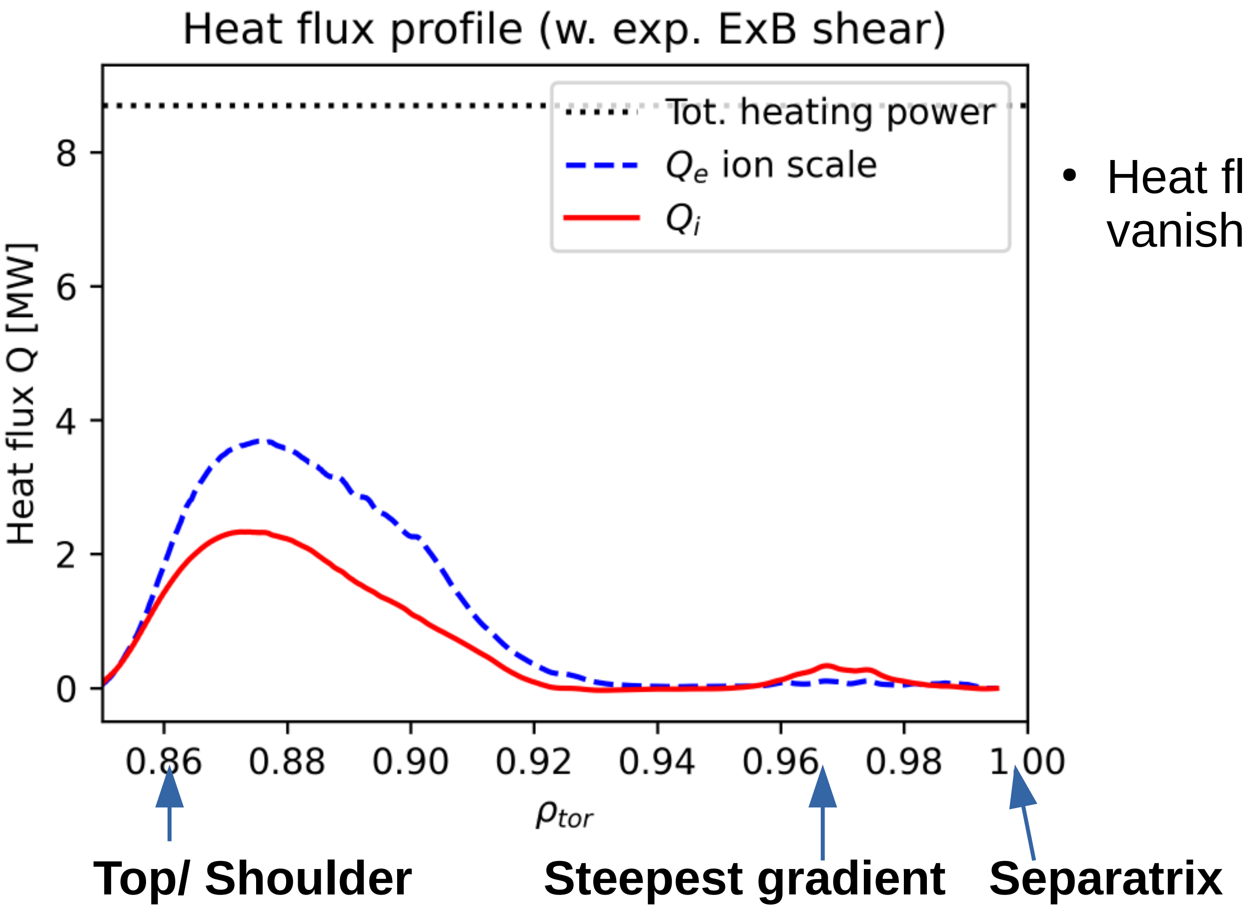

- Heat flux due to ion-scale fluctuations vanishes in pedestal center

Turbulent heat flux structure in pedestal

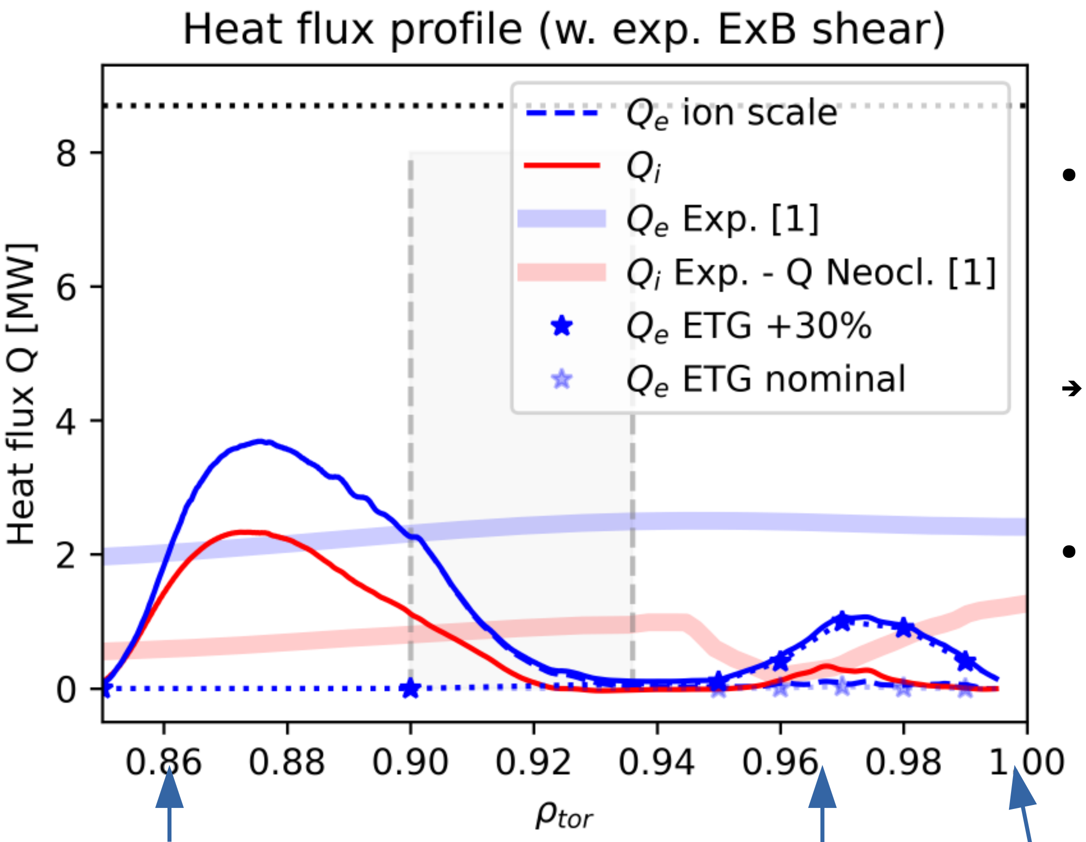

Top/ Shoulder **Steepest gradient** **Separatrix**

- Heat flux due to ion-scale fluctuations vanishes in pedestal center

➔ ETG takes over electron heat transport in steep gradient region from TEM at pedestal top

- ETG transport very sensitive to gradients (stiff profile)

[1] Viezzer et al., PPCF, 2020

Conclusions

I. **f-version upgrade of GENE code enables stable global, nonlinear, electromagnetic pedestal simulations**

II. **Transport in AUG #31529 pre-ELM pedestal is multi-channel & multi-scale:**
   - Electrostatic TEM with electromagnetic MTM contributions at pedestal top
   - ExB and mag. shear strongly suppress heat flux in all ion-scale channels
   - Dominant electron heat flux changes scale across pedestal: From TEM to ETG

→ Leppin et al., JPP, 2023, https://doi.org/10.1017/S0022377823001101

Part III: JET pedestal

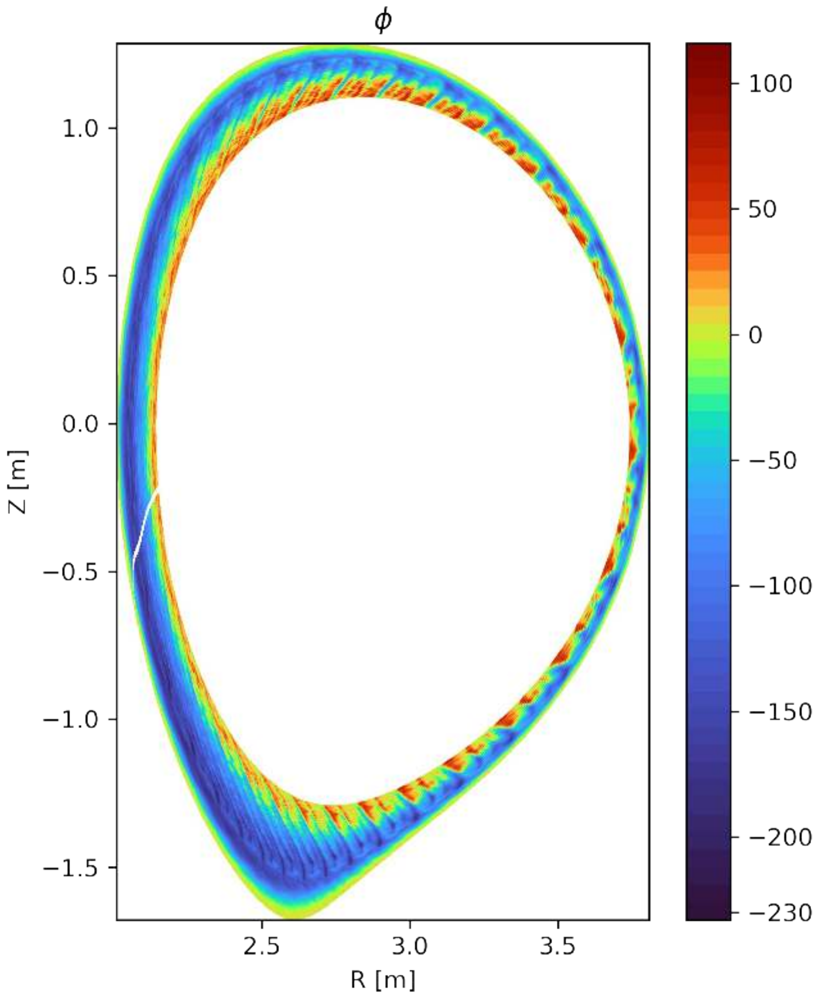

JET

ELMy H-mode pedestal from JET

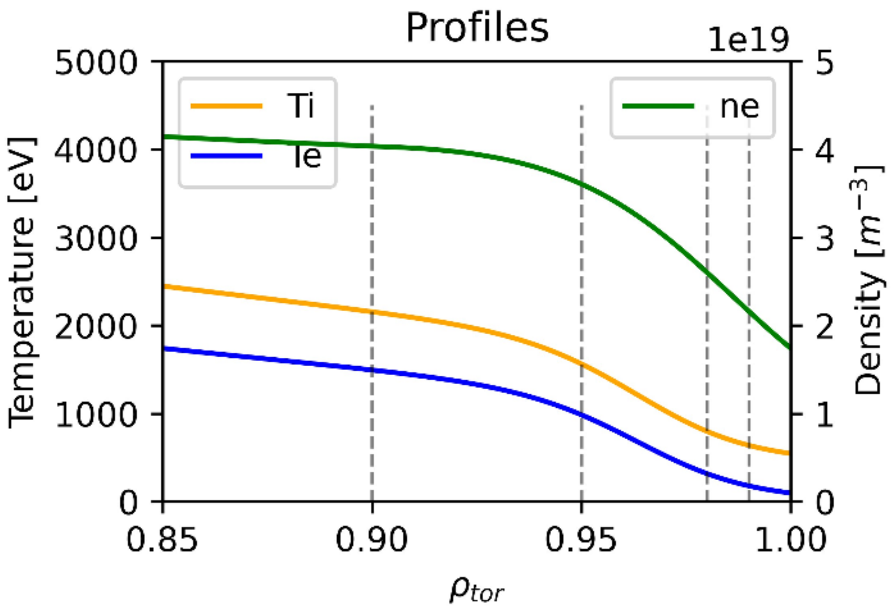

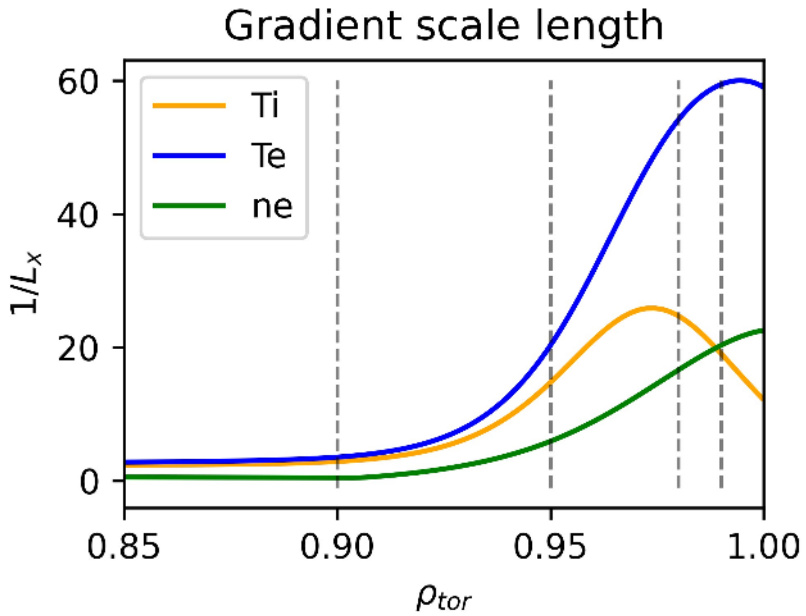

- ELMy H-mode JET #97781 (hybrid scenario, high beta)
- pre-ELM profiles
- P_{tot}= 33 MW

Linear instabilities

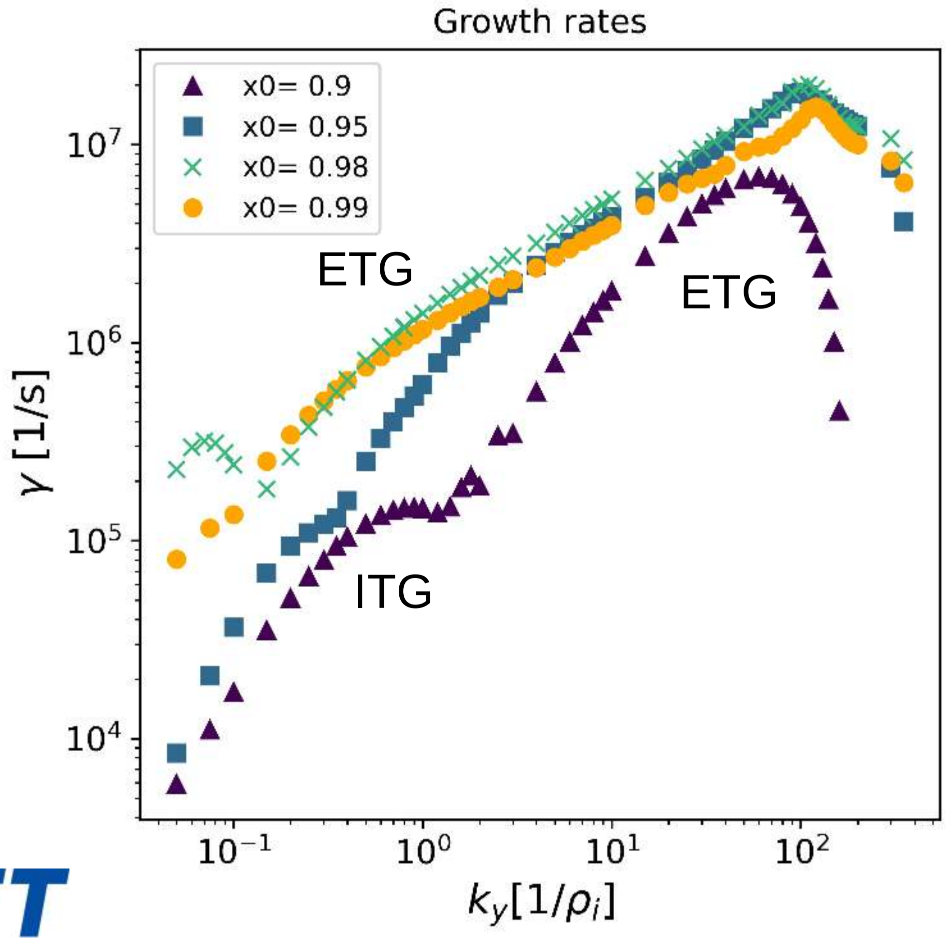

- Pedestal top:
  ITG (in contrast to TEM @ AUG)
  & ETG
- Pedestal center / foot:
  mostly ETG (extending to ion scales)
  small ITG-like peak
- ETG character (slab vs toroidal)
  depends on k_y and k_x i.e. ballooning angle
  (analysis ongoing)

  → see also recent studies by
  Chapman et al., Nucl. Fusion, 2022
  Parisi et al., Nucl. Fusion, 2020 / 2022

JET

Pedestal transport sensitive to ExB shear and impurities

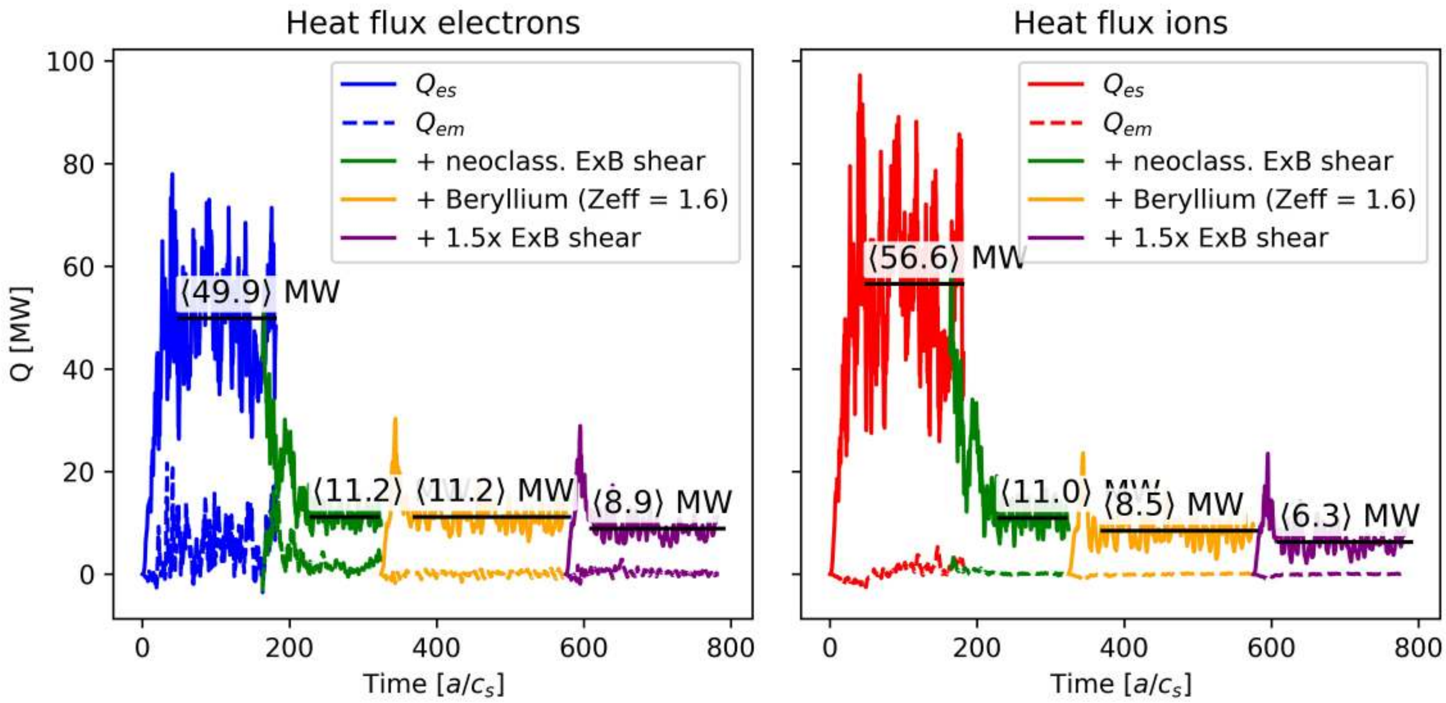

Radially averaged ρ_{tor} = 0.92 – 0.99

Global, nonlinear, 3 species GENE simulations

- Dominantly electrostatic heat flux
- increased relative ion heat flux in comparison to AUG
- ExB shear and impurities decisive in setting turbulent transport level

JET

Turbulent heat flux profile

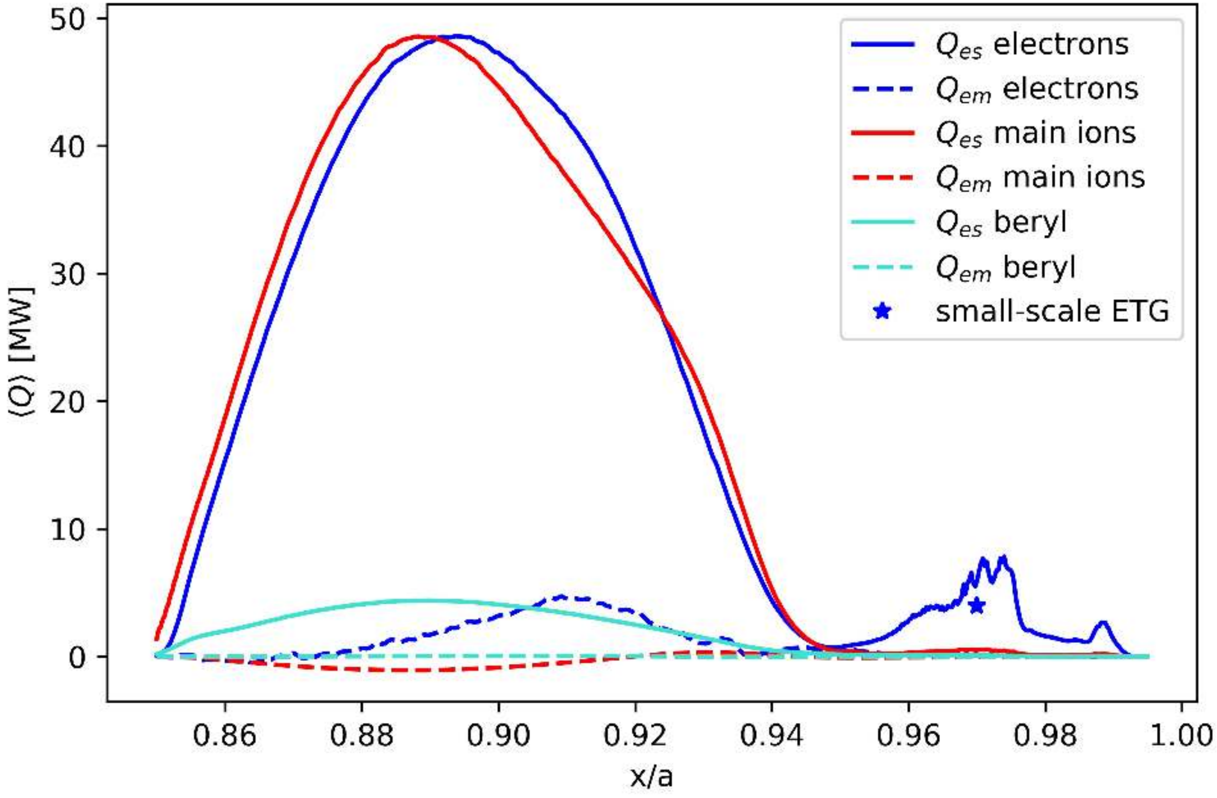

- Similar structure to AUG but smaller region of vanishing heat flux
- Electron heat flux in steep gradient region due to ion-scale fluctuations survives
- With current gradients unreasonably high peak heat flux in outer core
- Less ion heat flux in pedestal center than reported in Hatch et al., Nucl. Fusion, 2019

JET

Conclusions

I. **f-version upgrade of GENE code enables stable global, nonlinear, electromagnetic pedestal simulations**

II. **Transport in AUG #31529 pre-ELM pedestal is multi-channel & multi-scale:**
   - Electrostatic TEM with electromagnetic MTM contributions at pedestal top
   - ExB and mag. shear strongly suppress heat flux in all ion-scale channels
   - Dominant electron heat flux changes scale across pedestal: From TEM to ETG

→ Leppin et al., JPP, 2023, https://doi.org/10.1017/S0022377823001101

III. **Transport in JET #97781 pre-ELM hybrid H-mode pedestal:**
   - Dominant ITG contribution at pedestal top
   - Sensitive to ExB shear and impuritity level (turbulent ion-scale transport)
   - Non-vanishing electron heat flux by ion-scale fluctuations in pedestal center

MAX-PLANCK-INSTITUT
FÜR PLASMAPHYSIK

ASDEX Upgrade

Thank you for your attention!

E-mail: leonhard.leppin@ipp.mpg.de

EUROfusion

This work has been carried out within the framework of the EUROfusion Consortium, funded by the European Union via the Euratom Research and Training Programme (Grant Agreement No 101052200 — EUROfusion). Views and opinions expressed are however those of the author(s) only and do not necessarily reflect those of the European Union or the European Commission. Neither the European Union nor the European Commission can be held responsible for them.

JET ExB shear and impurities

V_{rot} due to E_r
(neoclassic approximation using D. Hatch script):

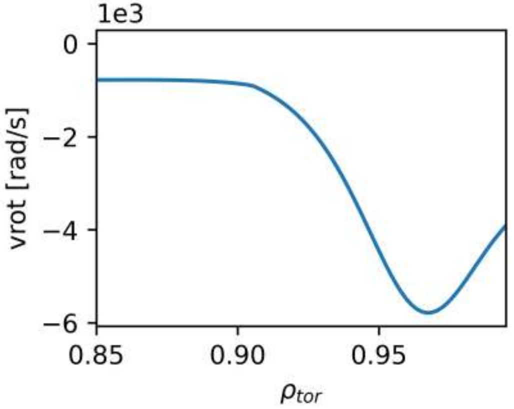

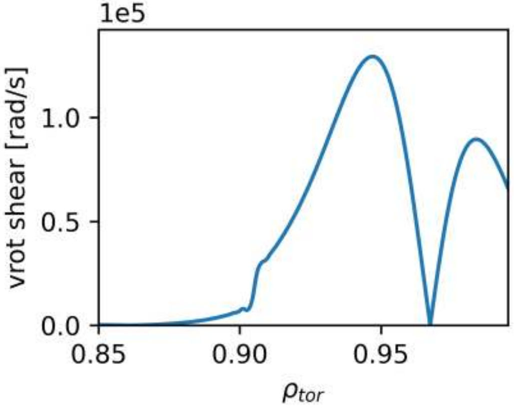

Some impurity variations within experimental uncertainty:

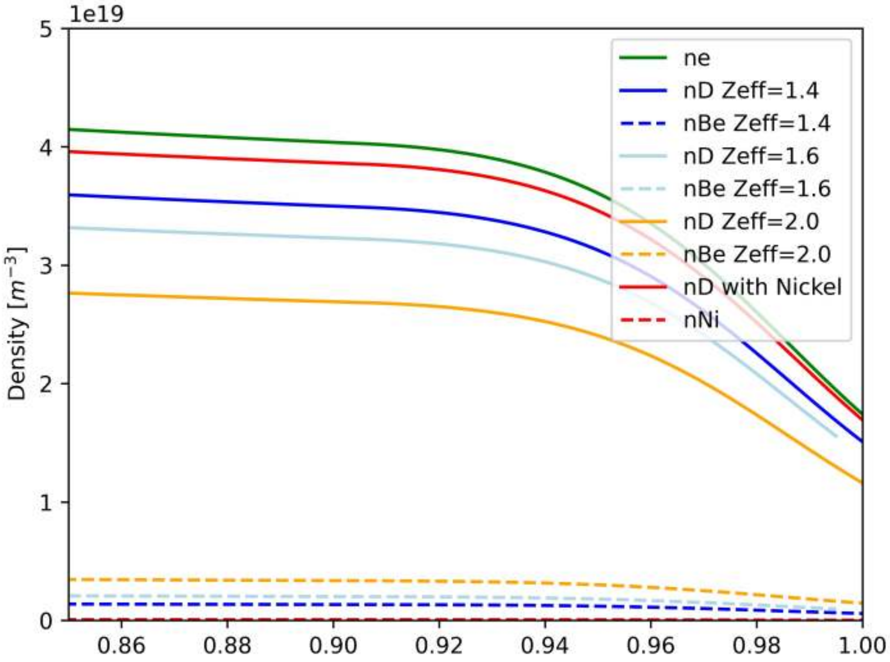

Focus on Be, because it has strongest main ion dilution for given Z_{eff}

JET

JET Impurities lower growth rates

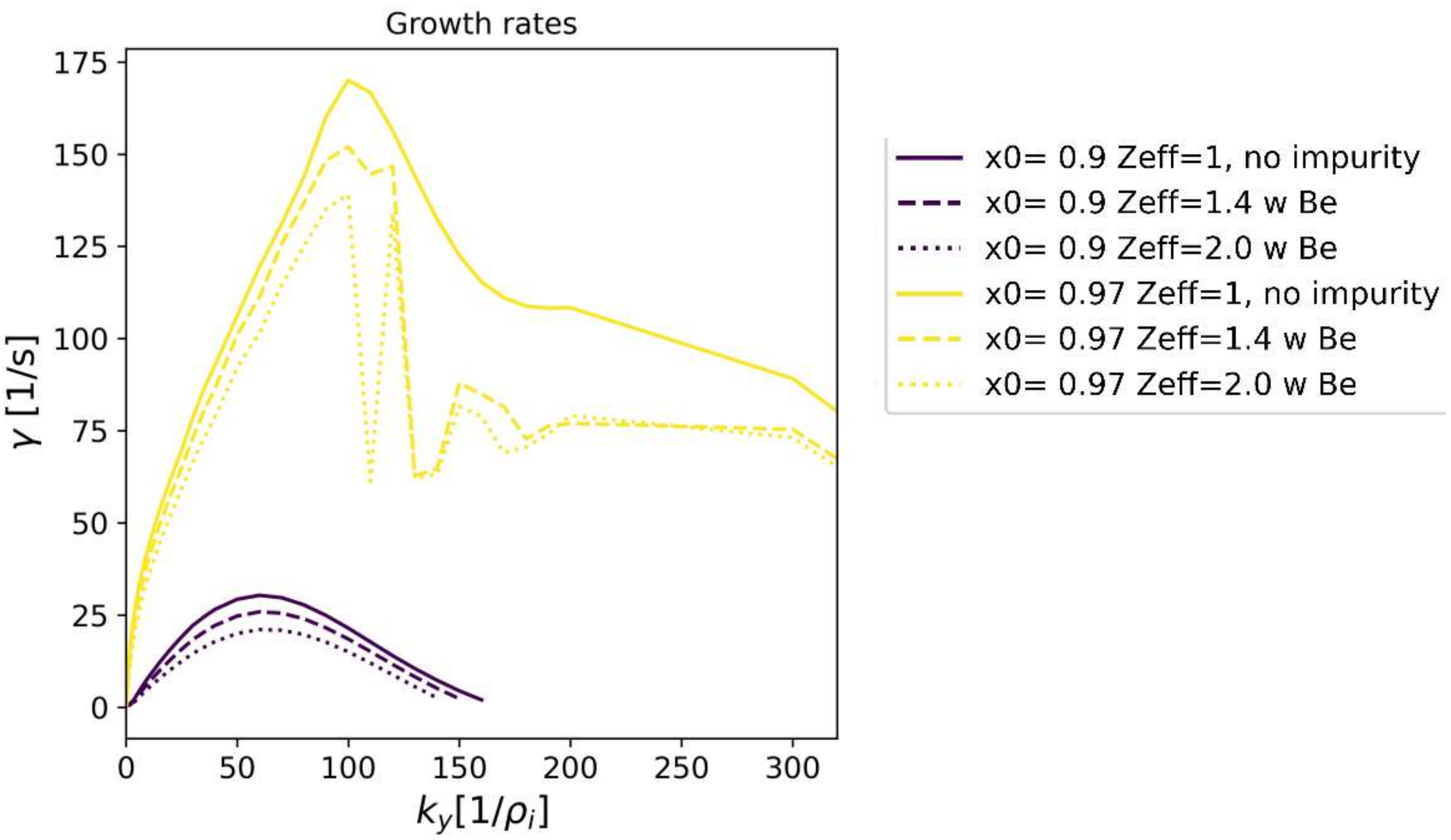

Other profiles JET

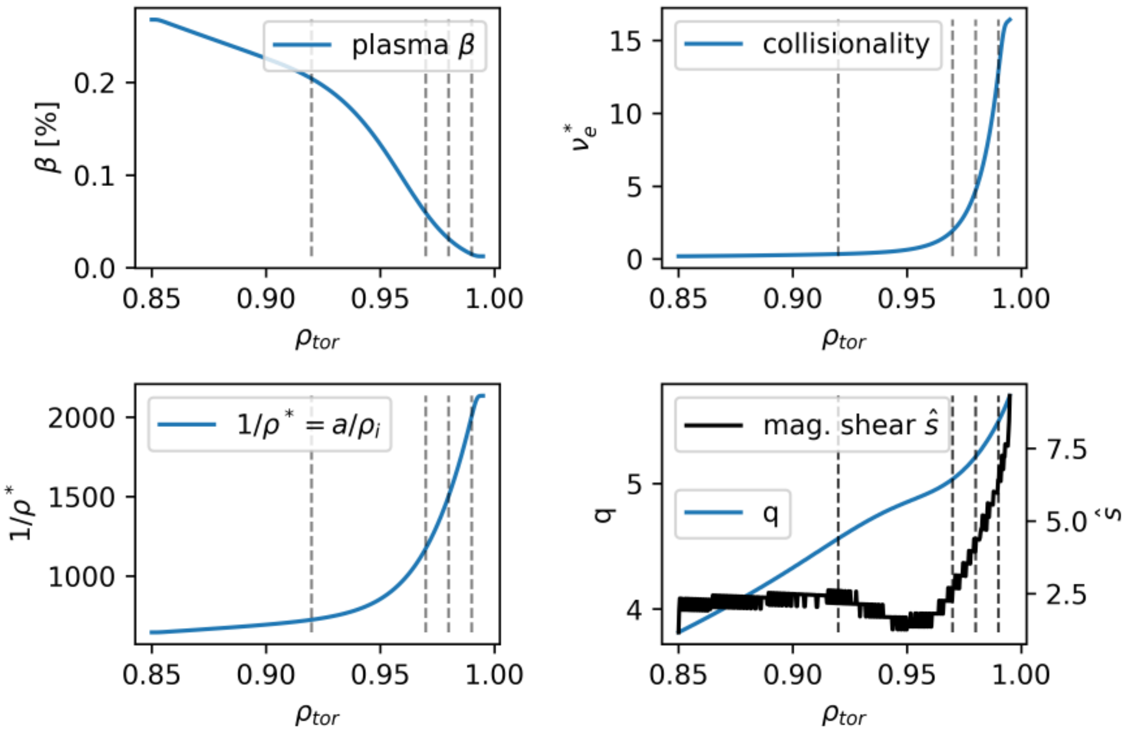

JET

Heat flux spectrum JET

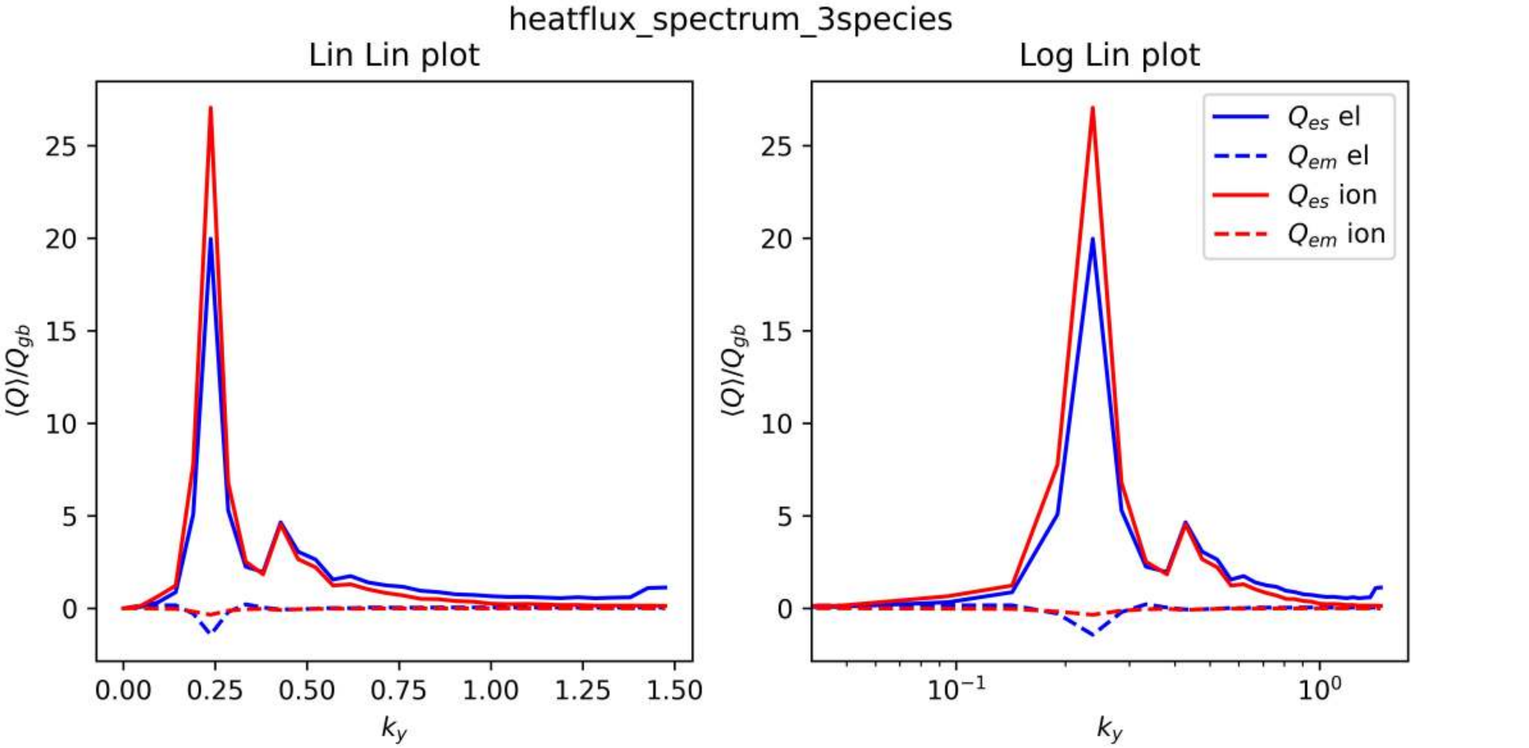

JET

ELMy H-mode pedestal from AUG

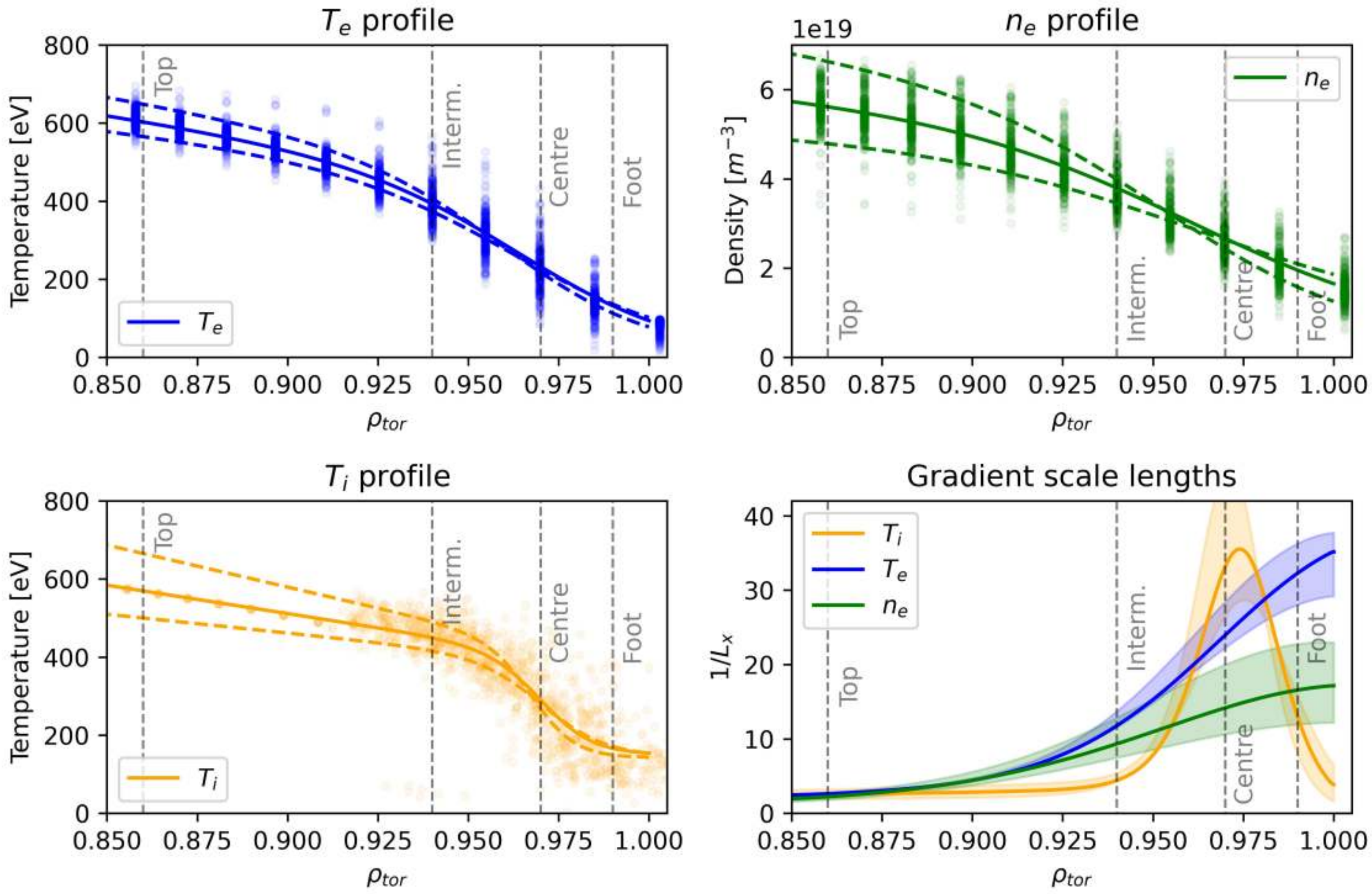

[1] Cavedon et al., PPCF, 2017

Heat flux spectrum AUG

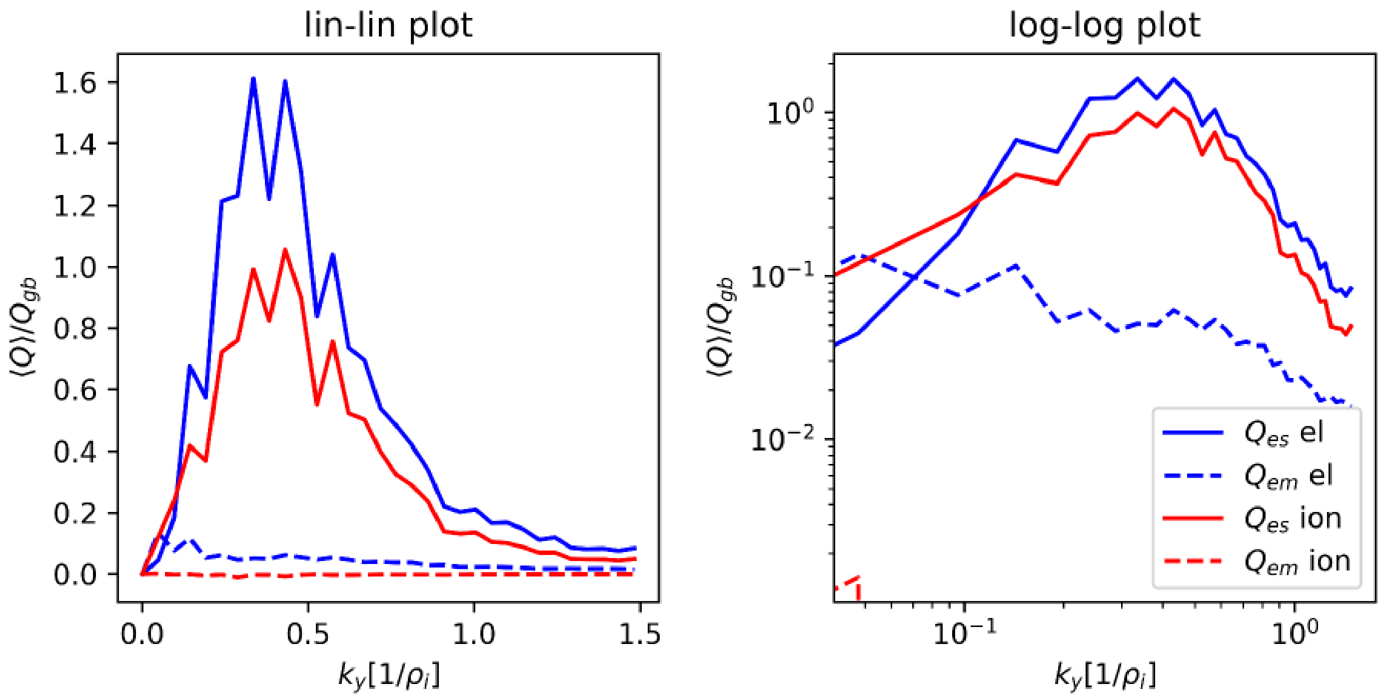

Full profiles AUG

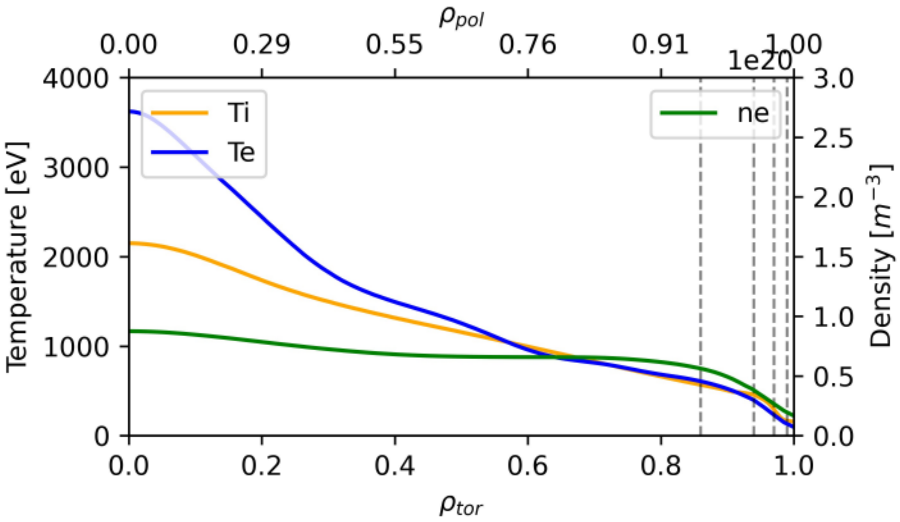

Zoom in:

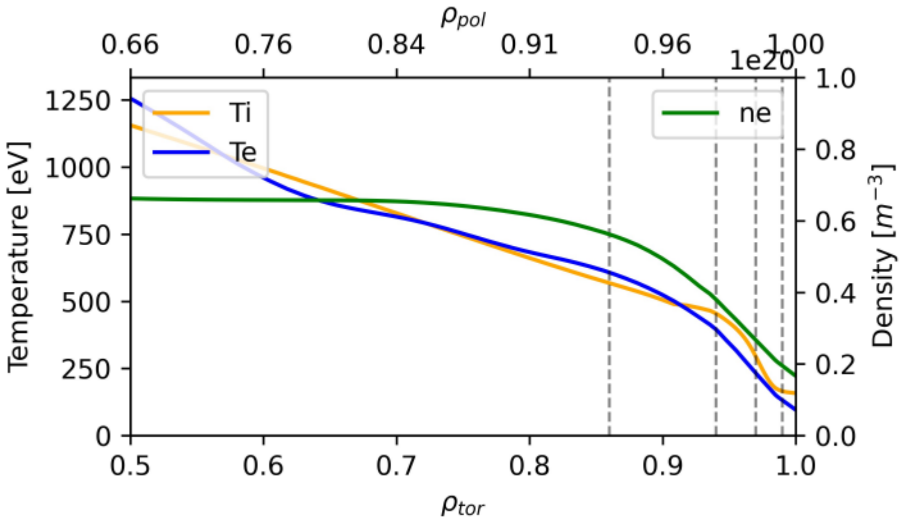

Other profiles AUG

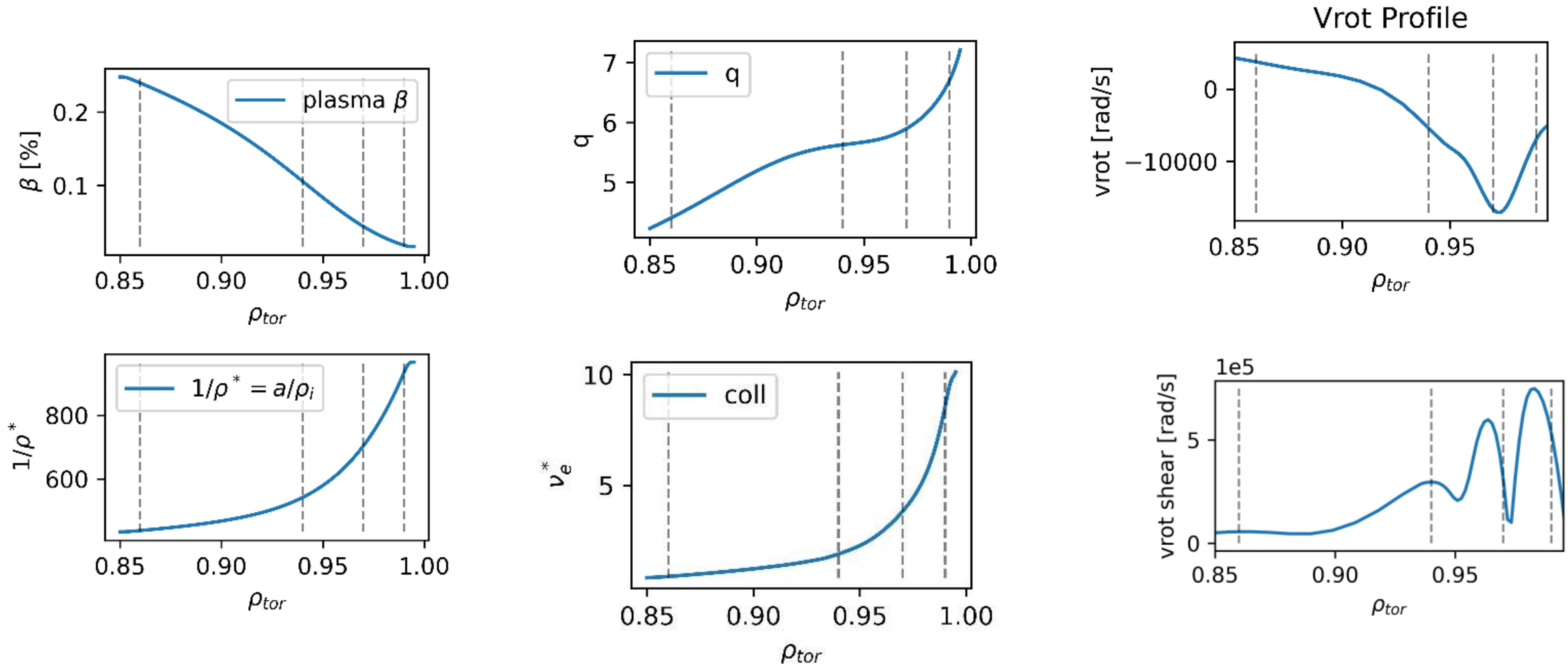

Close to linear KBM threshold

The pedestal is close to a linear KBM threshold. (In agreement with [4])
Distance decreases towards pedestal foot.

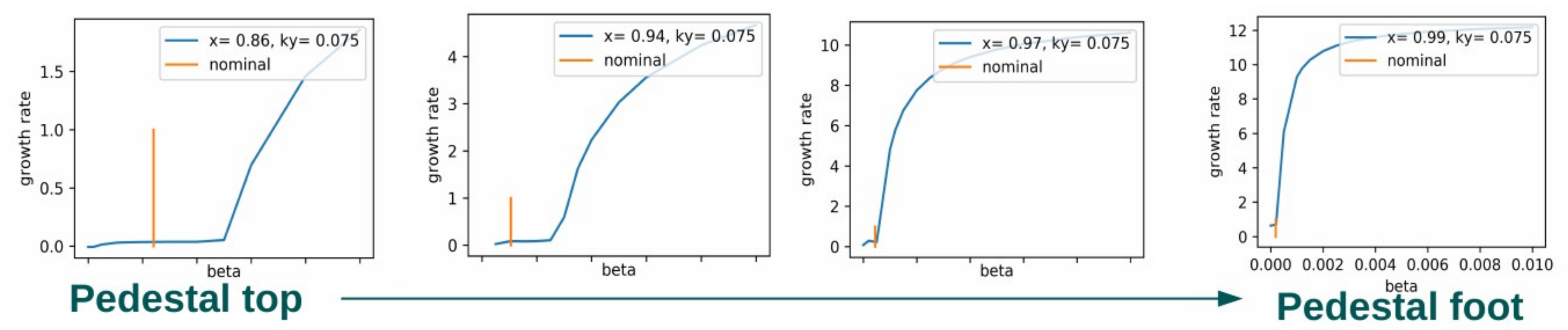

KBM: Kinetic Ballooning Mode

[4] Hatch et al, Nucl. Fus., 2015

Dangers of local, nonlinear simulations on ion-scales in pedestal center

Fluctuation contours

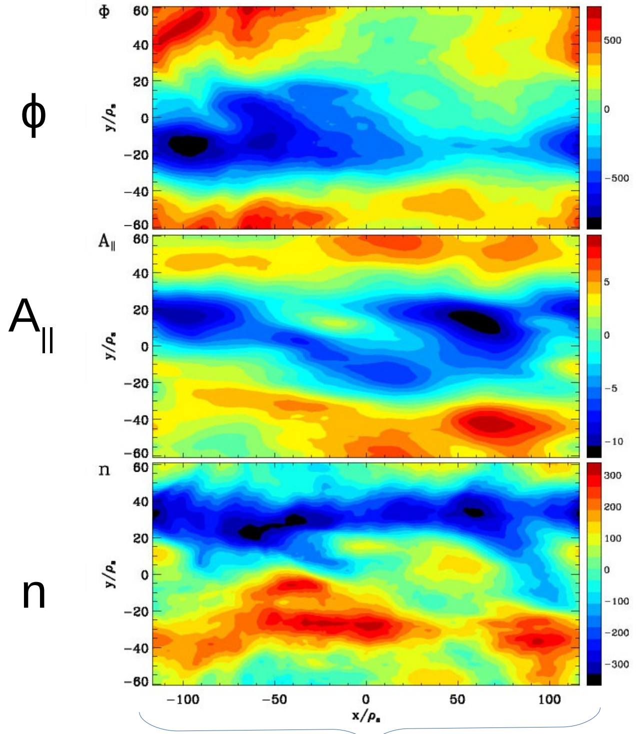

256 ρ_i

- short- circuiting of eddies across radial boundary condition, even for large boxes
  → heat flux not sensible

- high drive over large domain, even though in reality highly localized

For comparison: steep gradient ~ 25 ρ_i

AUG: Slab and toroidal ETG

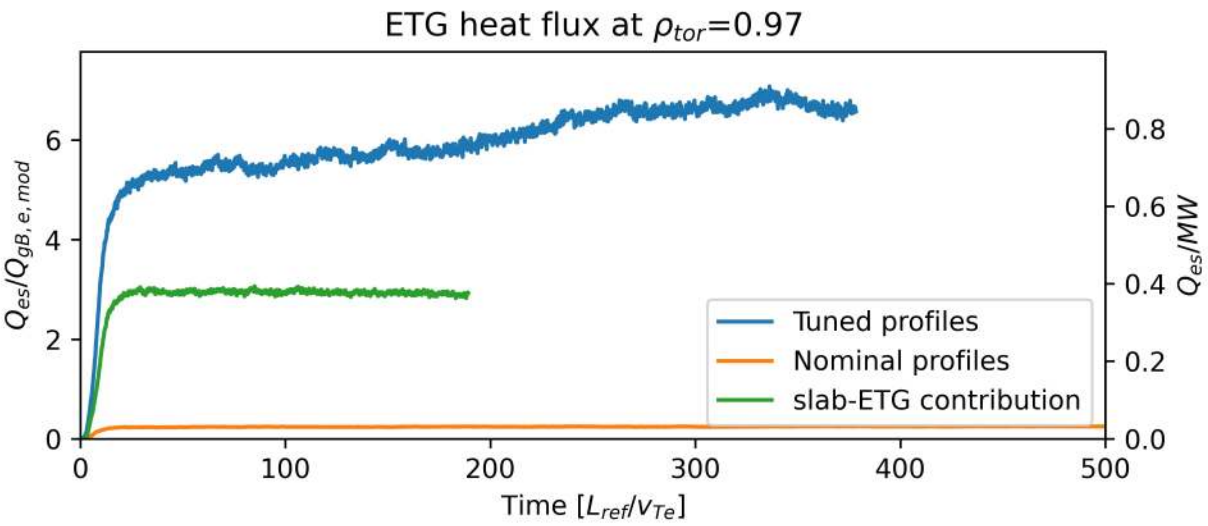

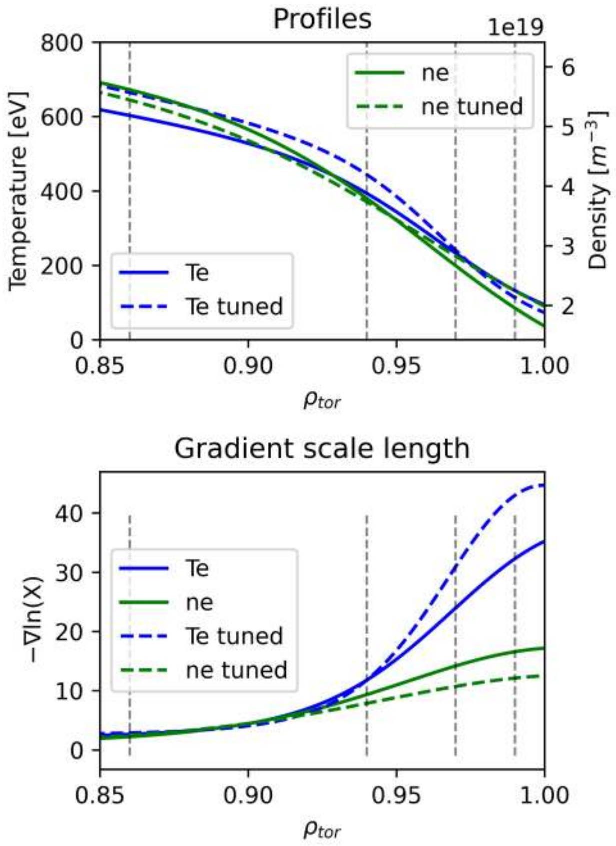

- high parallel resolution demand (nz > 200)

Simulation parameters Local, linear

6.1.1. *Linear, local simulations*

- 2 species, experimental β, realistic electron to ion mass ratio $m_e/m_D = 1/3670$, Landau collision operator. $E \times B$ shear was not used to avoid Floquet modes.
- Resolution: $n_x = 18$, $n_{ky} = 1$, $n_z = 36$, $n_v = 32$, $n_w = 16$.
- Box size: lv=3.1, lw=11.
- Convergence tests with increased parallel resolution ($n_z = 144$) and increased velocity space resolution ($n_v = 128$, $n_w = 32$) were performed.

Simulation parameters ETG nonlinear

6.2.2. *Nonlinear, local ETG simulations*

- 1 kinetic species (electrons), adiabatic ions, experimental β, Landau collision operator, no $E \times B$ shear.
- Resolution: $n_x = 512$, $n_{ky} = 64$, $n_z = 288$, $n_v = 32$, $n_w = 16$.
- Box size: lv=3, lw=9, lx=3.5.
- Convergence tests for radial resolution, radial box size and parallel resolution (up to nz=576) were performed for the position $rho_{tor} = 0.97$.

Simulation parameters global, nonlinear

6.1.3. *Nonlinear, global, ion scale simulations*

- 2 species, experimental β, realistic electron to ion mass ratio $m_e/m_D = 1/3670$, Landau collision operator. With $E \times B$ shear when indicated.
- Resolution: $n_x = 512$, $n_{ky} = 32$, $n_z = 48$, $n_v = 32$, $n_w = 16$.
- Box size: lv=3.45, lw=14.23, lx=72.
- Boundary conditions: Dirichlet with radial buffer zones (5% percent of domain at both boundaries), in which the distribution function is damped by fourth-order Krook operators.
- Performed with block-structured velocity grids (Jarema *et al.* 2017) with 4 blocks.
- Performed in single-precision floating-point format.

Validity of gyrokinetics in pedestal

Gyrokinetic derivation assumes small parameter ρ/L << 1:

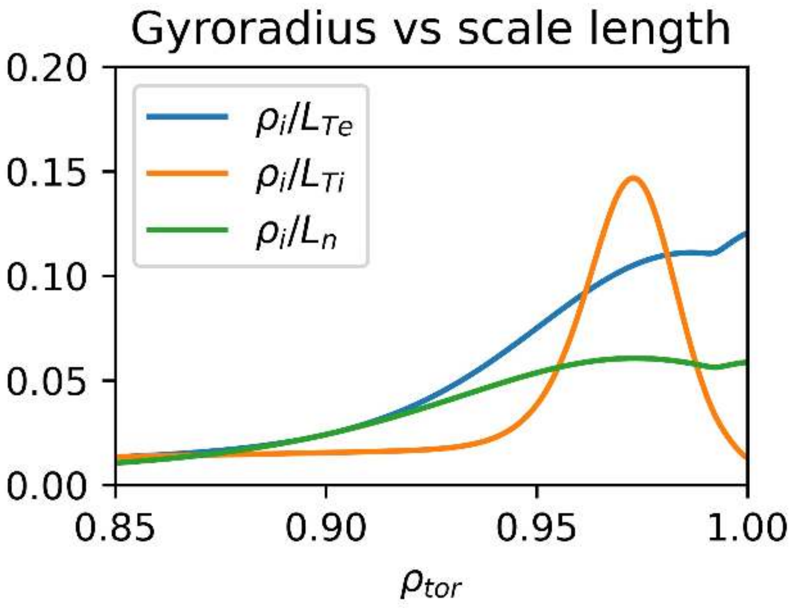

0.15 << 1 ? Still small enough?...